ICE VOLUMES ON CASCADE VOLCANOES:

MOUNT RAINIER, MOUNT HOOD, THREE SISTERS, AND MOUNT SHASTA

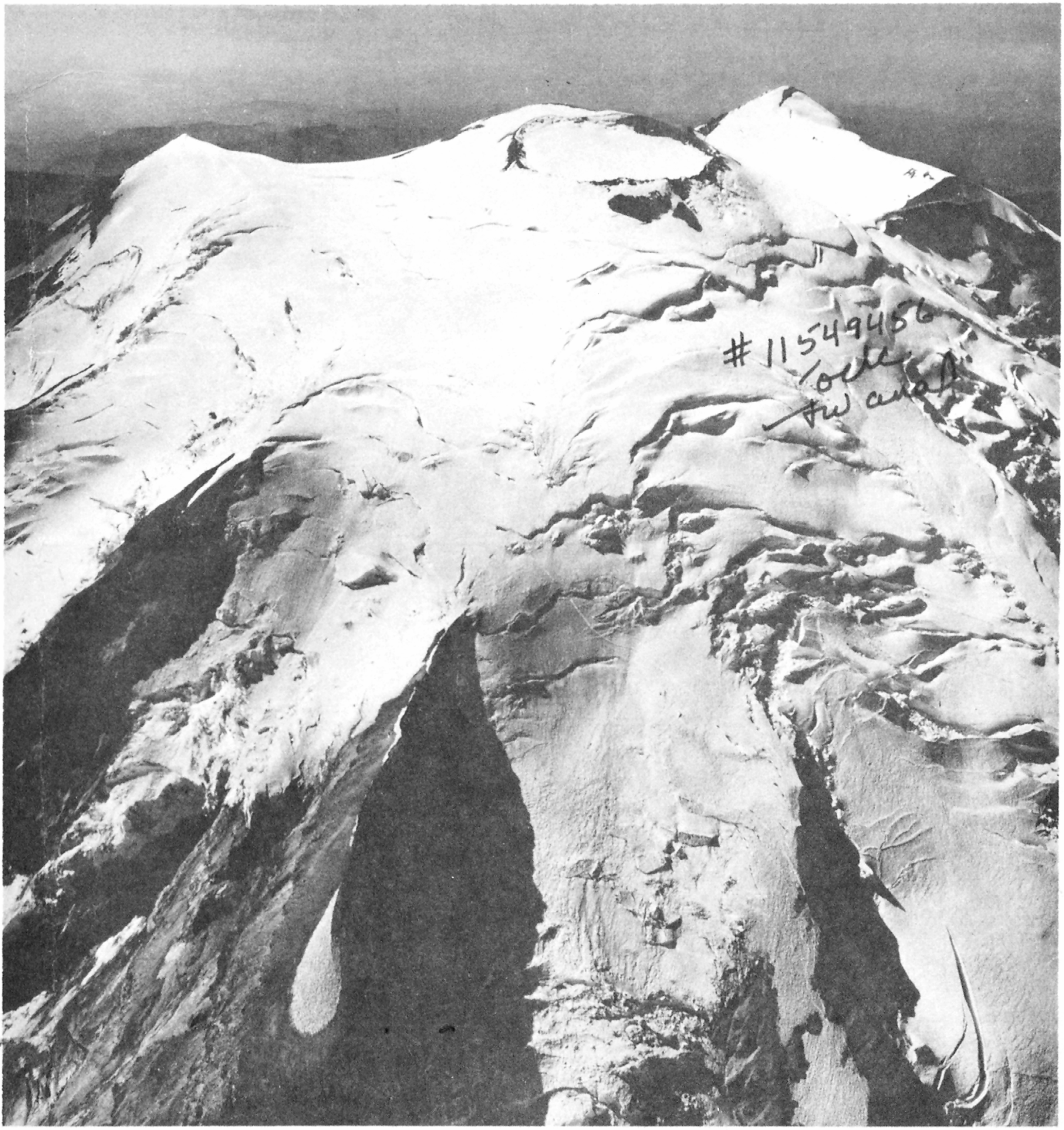

U.S. GEOLOGICAL SURVEY
Open-file Report 84-581

COVER: Mount Rainier from southeast. U.S. Geological Survey photograph by Austin Post, 1969.

UNITED STATES
DEPARTMENT OF THE INTERIOR
GEOLOGICAL SURVEY

ICE VOLUMES ON CASCADE VOLCANOES: MOUNT RAINIER, MOUNT HOOD, THREE SISTERS, AND MOUNT SHASTA

By C. L. Driedger[1] and P. M. Kennard[2]

U.S. GEOLOGICAL SURVEY

OPEN-FILE REPORT 84-581

[1]U.S. Geological Survey, Tacoma, WA
[2]U.S. Geological Survey, Tacoma, WA

Tacoma, WA
1984

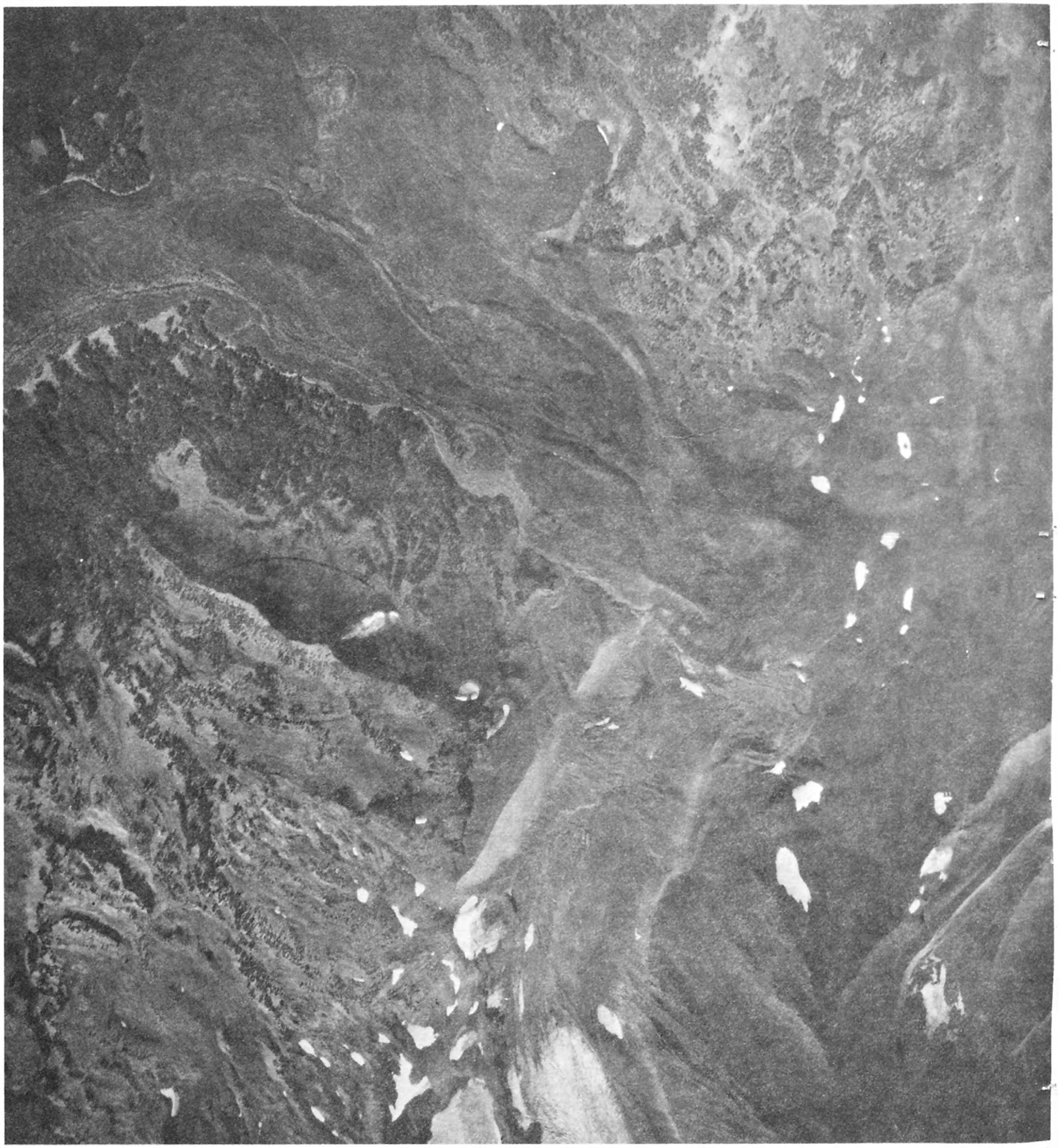

FRONTISPIECE.--Collier Cone (center of photograph), a cinder cone similar in eruption characteristics to the Mexican volcano Paricutin, was active between 500 and 2500 years B.P. (Taylor, 1981, p. 61) and erupted between the lateral moraines of Collier Glacier. During the early 1930's the terminus of Collier Glacier abutted the south flank of Collier Cone, reworking the cinders into the striated pattern visible today (Ruth Keen, Mazamas Mountaineering Club, oral communication, 1984). Williams (1944) reported the presence of glacial moraine interspersed with lava flows around the base of Collier Cone. U.S. Geological Survey photograph by Austin Post on September 9, 1979.

UNITED STATES DEPARTMENT OF THE INTERIOR

William P. Clark, Secretary

GEOLOGICAL SURVEY

Dallas L. Peck, Director

For additional information write to:

U.S. Geological Survey
Project Office - Glaciology
1201 Pacific Avenue, Suite 450
Tacoma, Washington 98402

CONTENTS

ABSTRACT 1

INTRODUCTION - PURPOSE AND SCOPE 1

ACKNOWLEDGEMENT 3

FIELD MEASUREMENTS 3

PRIMARY DATA REDUCTION 5

Migration 8

Use of maps and photographs 9

Surface features and their relation to the basal topography 9

Isopach maps as interpretive tools 14

DETERMINATION OF VOLUMES 14

Measured glaciers 14

Unmeasured glaciers and snow patches 15

RESULTS 20

Mount Rainier 20

Mount Hood 25

Three Sisters 31

Mount Shasta 38

CONCLUSIONS 42

APPENDIX 45

REFERENCES CITED 53

ILLUSTRATIONS

Cover.--Mount Rainier from southeast. U.S. Geological Survey photograph by Austin Post, 1969..

Frontispiece.--Photograph of Collier Glacier moraine abutting Collier Cone near the Three Sisters, Oregon. U.S. GeologicalSurvey photograph....................

Plate 1-6B.--Map showing:
1.--Mount Rainier basal and surface contours...............in pocket
2.--Mount Rainier isopachs on glaciers measured by ice radar..in pocket
3.--Mount Hood basal and surface contours.................in pocket
4.--Three Sisters basal and surface contours...............in pocket
5.--Mount Hood and Three Sisters isopachs on glaciers measured by ice radar...............................in pocket
6A.--Mount Shasta basal and surface contours...............in pocket
6B.--Whitney Glacier isopachs..............................in pocket

Figure 1.--Index map showing location of volcanoes in study areas............ 2
2.--Photograph showing ice radar equipment used during study.......... 4
3.--Scheme of interactive process to produce basal maps............... 6
4.--Diagrams showing:
A.--Location of transmitter and reciever......................... 7
B.--Geometry of radar to relection and migration procedure........ 7
5.--Photographs of:
A.--Nisqually Glacier, 1944.......................................10
B.--Nisqually Glacier, 1980.......................................11
6.--Rock avalanche debris concealing glacier ice on Lost Creek Glacier, Soth Sister, Oregon.......................................12
7.--Diagram of a volume element...13
8.--Photograph of Mount Rainier, Washington.............................21
9.-11.--Mount Rainier graphs showing:
9.--Ice and snow area by altitude....................................22
10.--Ice volume by altitude on glaciers measured with ice radar........23
11.--Ice area by thickness..24
12.--Photograph of Mount Hood, Oregon.....................................26
13-15.--Mount Hood graphs showing:
13.--Ice and snow area by altitude...............................27
14.--Ice volume by altitude on glaciers measured with ice radar...29
15.--Ice area by thickness.......................................30
16.--Photograph of the Three Sisters, Oregon..........................34
17-19.--Three Sisters graphs showing:
17.--Ice and snow area by altitude...............................35
18.--Ice volume by altitude on glaciers measured with ice radar...36
19.--Ice area by thickness.......................................37
20.--Photograph of Mount Shasta, California...........................39
21-23.--Mount Shasta graphs showing:
21.--Ice and snow area by altitude...............................41
22.--Ice volume by alittude on glaciers measured with ice radar...43
23.--Ice area by thickness.......................................44

24-27.-- Diagrams showing:
24.--Schematic of radar system....46
25.--Antenna detail....48
26.--Oscilloscope output....50
27.--Typical antenna configurations....51

TABLES

Table 1.--Glacier lengths, basal shear stresses, and voluem estimation applications....16
2.-5.--Areas and volumes of glacier ice and snow at:
2.--Mount Rainier....19
3.--Mount Hood....28
4.--Three Sisters....32
5.--Mount Shasta....40

Conversion Factors

For readers who prefer International System Units (SI), conversion factors for terms used in this report are listed below. Except where required by use with maps, stresses are expressed in bars (10^5 Pascals), a preferred unit in Glaciology.

Multiply US Inch/Pound Units	By	To obtain SI
foot (ft)	0.3048	meter (m)
square foot (ft^2)	0.0929	square meter (m^2)
cubic foot (ft^3)	0.0283	cubic meter (m^3)
mile (mi)	1.609	kilometer (km)
square mile (mi^2)	2.590	square kilometer (km^2)
cubic mile (mi^3)	4.168	cubic kilometer (km^3)
pounds per square foot (lb/ft^2)	4.787×10^{-4}	bar
slug per cubic foot ($slug/ft^3$)	1.187	kilogram per cubic meter (kg/m^3)

Water equivalence:

$$\text{Volume of water in cubic feet} = \frac{(\text{Volume of ice in cubic feet } (1.8 \text{ slugs/ft}^3)}{1.94 \text{ slugs/ft}^3}$$

In this study, inch-pound units have been used because of compatibility with the most current Geological Survey topographic maps.

SYMBOLS AND ABBREVIATIONS

Symbol	Name
A	Surface area
b	Slope of bedrock measured from horizontal
c	Speed of light in ice
c_o	Speed of light in a vacuum
CI	Contour interval
d	Transmitter-receiver separation distance
g	Gravitational acceleration
h	Thickness measured perpendicular to the reflecting point on a glacier bed
h'	Vertical distance between the measurement point and the bedrock
i	(Subscript) indicates an interval value
$K_{1,2,3}$	Coefficients derived from regression analysis
l	Glacier length
p	Path of light
R	Resistance per unit length
t	Time between arrivals of air and reflected waves on the oscilloscope
V	Volume
V*	Volume estimation by calculation of basal shear stress
x	Distance from antenna feedpoint in meters
α	Slope of ice measured from horizontal
ℓ	Antenna half-length (meters)
η	Refractive index of ice
ν	Frequency
ρ	Density of ice
τ	Basal shear stress
τ^*	Estimated basal shear stress
ψ	Resistive loading constant (ohms)

ICE VOLUMES ON CASCADE VOLCANOES: MOUNT RAINIER, MOUNT HOOD, THREE SISTERS, AND MOUNT SHASTA

By Carolyn L. Driedger[1] and Paul M. Kennard[2]

ABSTRACT

During the eruptions of Mount St. Helens the occurrence of floods and mudflows made apparent the need for predictive water-hazard analysis of other Cascade volcanoes. A basic requirement for such analysis is information about the volumes and distributions of snow and ice on other volcanoes.

A radar unit contained in a backpack was used to make point measurements of ice thickness on major glaciers of Mount Rainier, Washington; Mount Hood, Oregon; the Three Sisters, Oregon; and Mount Shasta, California. The measurements were corrected for slope and were used to develop subglacial contour maps from which glacier volumes were measured.

These values were used to develop estimation methods for finding volumes of unmeasured glaciers. These methods require a knowledge of glacier slope, altitude and area, and an estimation of basal shear stress, with each derived using topographic maps updated by aerial photographs. The estimation methods were found to be accurate within $\pm$ 20 percent on measured glaciers, and to be within $\pm$ 25 percent when applied to unmeasured glaciers on the Cascade volcanoes. The estimation methods may be applicable to other temperate glaciers in similar climatic settings.

Areas and volumes of snow and ice are as follows: Mount Rainier 991 million ft^2, 156 billion ft^3; Mount Hood 145 million ft^2, 12 billion ft^3; Three Sisters 89 million ft^2, 6 billion ft^3; and Mount Shasta 74 million ft^2, 5 billion ft^3.

The distribution of ice and firn patches within 58 glacierized basins on volcanoes are mapped and listed by altitude and by watershed to facilitate water hazard-analysis.

INTRODUCTION

The 1980 eruptions of Mount St. Helens removed an estimated 4.6 billion ft^3 of ice and snow from the mountain aiding the formation of lahars and floods (Brugman and Post, 1981, p. D1). There is evidence of similar glaciovolcanic interactions on other Cascade volcanoes and man can anticipate such threats during future eruptions. Therefore, determining the volumes of the ice and snow should be useful in assessing the potential hazard from eruptions of individual volcanoes.

Between April and September 1981 an ice-radar system developed by the U.S. Geological Survey was used to determine ice thickness at 177 measurement points on 25 glaciers of Mounts Rainier, Hood, and Shasta, and the North, Middle, and South Sisters (collectively referred to here as the Three Sisters, fig. 1).

[1]U.S. Geological Survey, Tacoma WA
[2]U.S. Geological Survey, Tacoma WA

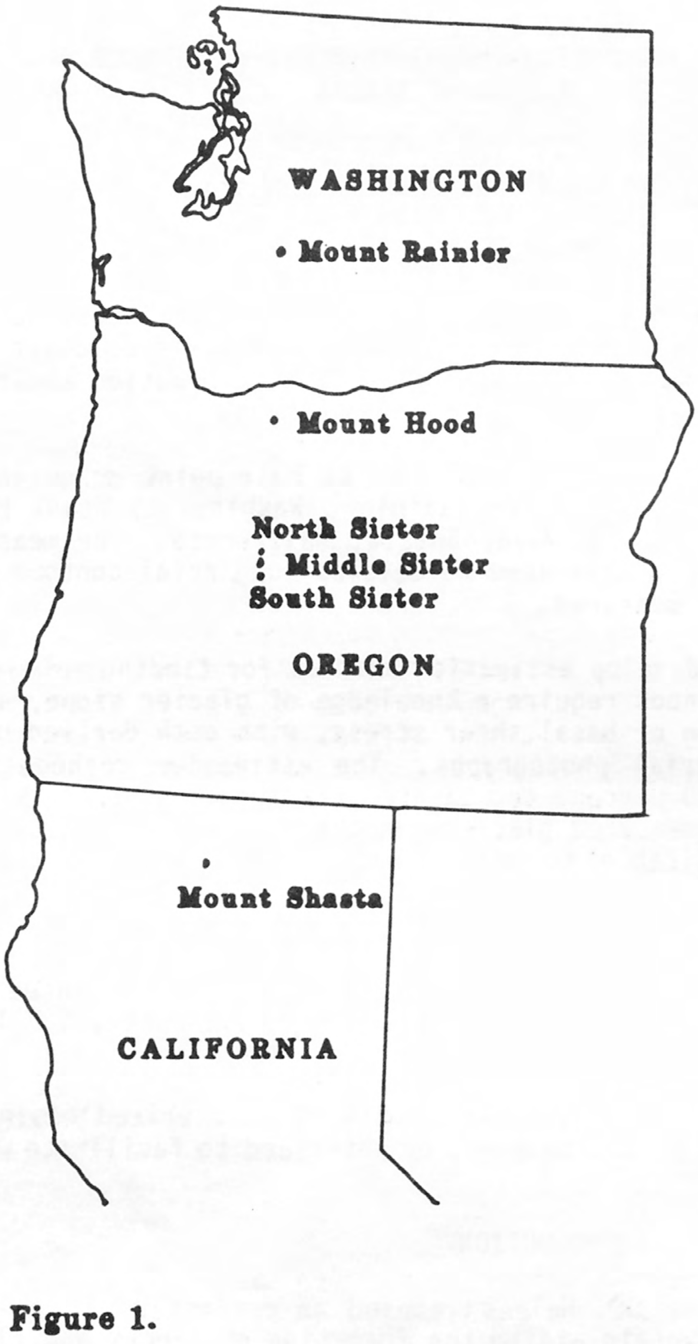

Figure 1.--Locations of volcanoes studied.

Access to these measurement points was by foot, ski, and helicopter, and involved personnel from the Project Office - Glaciology, Tacoma, Wash. The measurements allowed the preparation of subglacial contour and isopach maps which are included in this paper, along with the resulting volume calculations. The descriptions of ice-radar operation and methods for data reduction, calculation of glacier volume, and error totals calculating glacier volume are condensed from a study by Kennard (1983).

ACKNOWLEDGMENTS

Suzanne Brown, Lee Benda, David Peckham, Melinda Brugman and others from the U.S. Geological Survey Project Office - Glaciology and from the Cold Regions Hydrology Project provided invaluable help during this study. During the 6 months of fieldwork, they aided with radar measurements and surveying, and by giving their constant energy and enthusiasm. Success in making measurements in nearly inaccessable places was often due to support by Sue and Anthony Reece of HiLine Helicopters.

Personnel of Mount Rainier National Park, and of the Mount Hood, Deschutes, Willamette, and Shasta National Forests cooperated by providing information on mountain conditions and by allowing the use of necessary logistics within these regions.

Dr. Charles Raymond offered valuable insight and support for developing the volume estimation methods.

Paul Kennard organized and coordinated fieldwork for the study. He determined the basal contours for the Mount Rainier and Mount Hood glaciers and later developed the volume estimation methods and error analysis discussed here. Carolyn Driedger and Bruce Vaughn determined the basal contours at the Three Sisters and Mount Shasta. They applied the estimation methods to all unmeasured glaciers noted in the study.

Beneficial reviews of the manuscript were made by Dee Molenaar, Bernard Hallet, and Robert Jacobel. William Scott, C. Dan Miller, and Dwight Crandell provided information and sectional reviews in reference to geologic histories and glaciovolcanic relationships.

This report was prepared by Carolyn Driedger. The Appendix was prepared by Paul Kennard.

FIELD MEASUREMENTS

The work schedule required use of portable, monopulse-radar equipment that could be deployed rapidly from a backpack, and needed use of antennas applicable to a wide range of ice thickness. In the radar operation, separate transmitting and receiving antennas were placed on the ice a known distance apart. An oscilloscope recorded arrival of the transmitted air wave and the wave reflected from the bedrock (fig. 2). Oscilloscope screen output was photographed on self-developing film. The theory and principles of operation of the monopulse radar are described in more detail in the Appendix.

Figure 2.--Ice radar unit in operation on Diller Glacier on the Middle Sister, Oregon. Transmitter with antennas is on the snow. Receiving unit and oscilloscope are operated from top of backpack. U.S. Geological Survey photograph by Carolyn Driedger in September 1981.

As all depth measurements were point measurements, it was necessary to obtain accurate map positions, and, as large ice masses have few features identifiable with certainty on a map, surveying was required on Mount Rainier and Mount Hood. Standard survey procedures were followed for field surveying, using a theodolite and an electronic distance-measuring device. Because glaciers on the Three Sisters and Mount Shasta are generally smaller than those on Mounts Hood and Rainier, locations could be determined adequately with a pocket transit and aerial photos.

Measurement points were selected to give representative coverage of the major ice bodies on each mountain, as well as on some smaller glaciers and patches of perennial snow (firn), referred to in this paper as snow patches.

The number of measurement points on each glacier ranged from 1 to 31. The ultimate number and locations were determined by weather, avalanche and icefall conditions, suitable helicopter landing areas, and the ability to obtain unambiguous bottom measurement returns. Final data-point locations are shown on plates 1-6 (back pocket).

Primary Data Reduction

The iteration of processes required for developing bedrock and isopach maps is detailed here, and is summarized in figure 3. The first step following fieldwork involves finding the ice thickness at each measurement point. Figures 4a and 4b show the geometry of a measurement point and indicate the path of the radar wave between bedrock and the surface. The procedure uses equation 1, where it is assumed that the glacier and bedrock surfaces are planar and the glacier consists only of ice.

Required for the calculation are the separation distance between the pulse source and the receiver (d), the time interval between the arrival at the oscilloscope of the air wave and the reflected wave, the speed of light in a vacuum (c_0) and the refractive index of ice (η). An apparent thickness h was calculated at each point by

$$h = \frac{\left[\left(\frac{c_0}{\eta} t + \frac{d}{\eta}\right)^2 + d^2\right]^{1/2}}{2} \tag{1}$$

Computations showed that correcting for the differences in the refractive index of ice, firn, and snow had an effect of less than two and a half percent on glacier-thickness determinations because the layers of snow and firn are thin. In the data reduction, the presence of snow and firn were disregarded and the total thickness at each measurement point was assumed to be ice. Any debris-laden layer at the base of the ice was assumed to be a reflecting surface and was considered glacier bed.

Thickness measurements were considered accurate to $\pm$ 3.0 percent for a typical data point, including photograph reading errors and errors owing to neglecting the presence of snow and firn. These apparent point thicknesses, together with geological interpretation, were used to develop subglacial contour maps, referred to hereafter as basal maps.

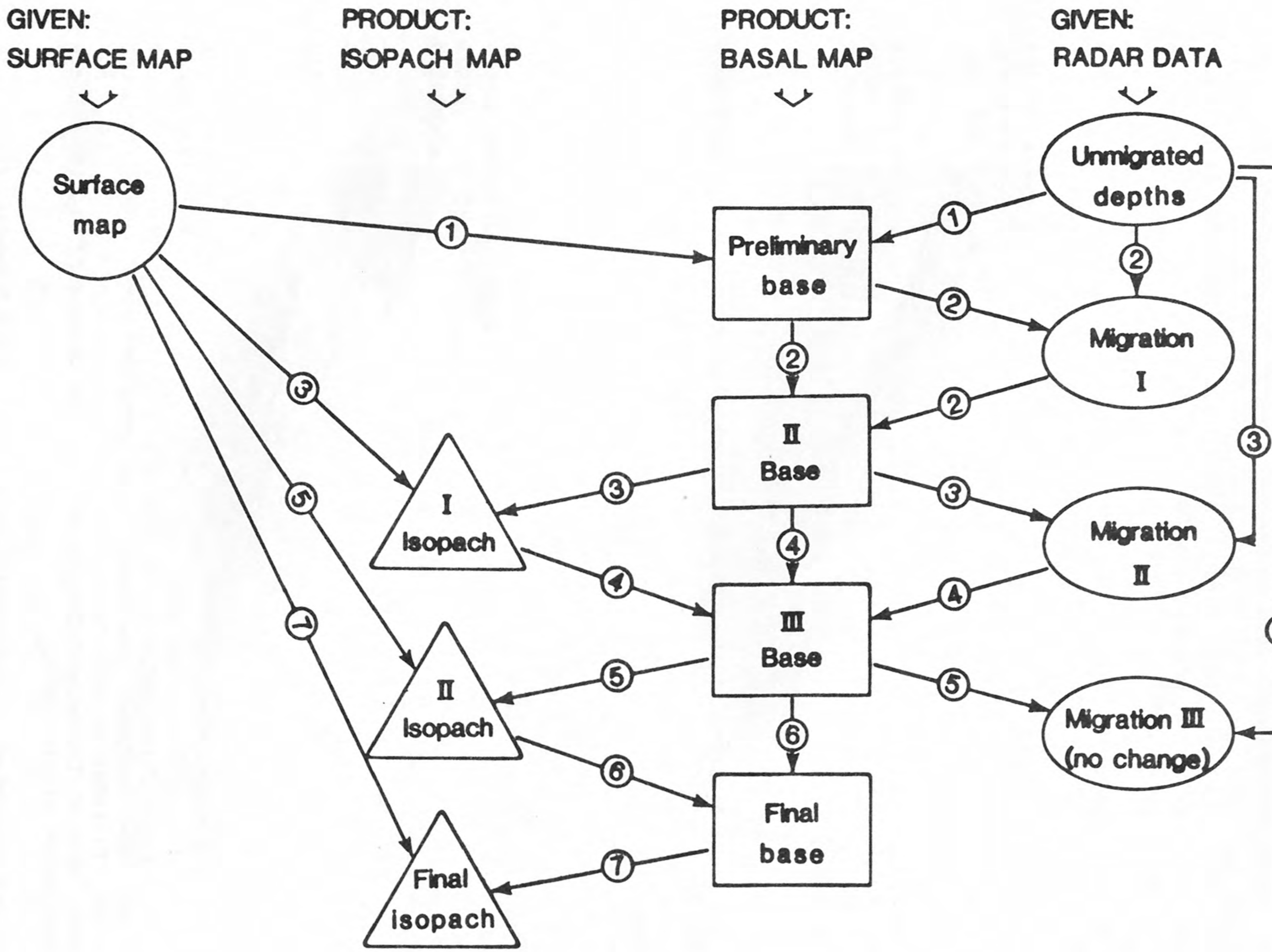

Figure 3.

Figure 3.--Interactive processes used to produce basal and isopach maps, as in plates 1 through 6 (Kennard, 1983).

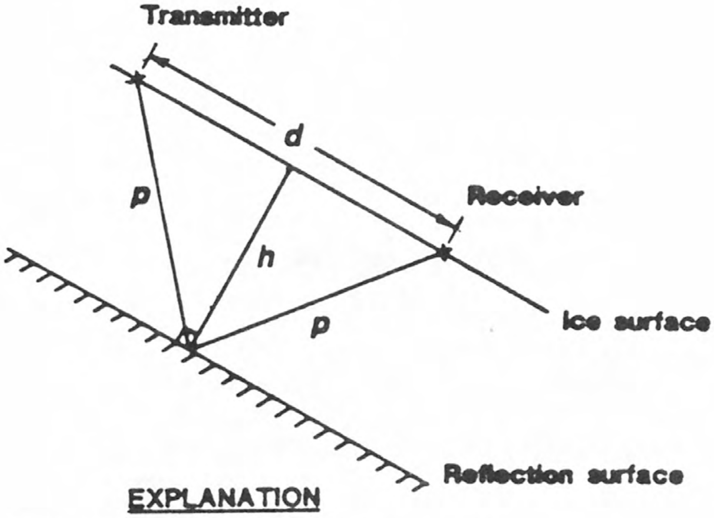

EXPLANATION

2*p* = Pathlength of the reflected wave

d = Transmitter–receiver separation distance

h = Unmigrated thickness

Figure 4a.

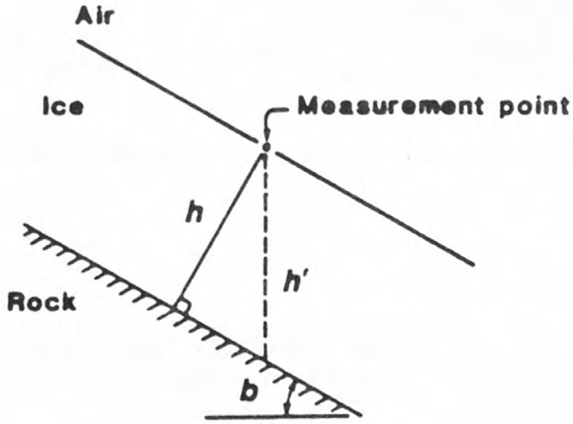

EXPLANATION

• = Measurement point–source receiver midpoint

h = Unmigrated thickness

h' = Migrated thickness

b = Slope of basal plane

Figure 4b.

Figure 4A-B--Figure 4A indicates the locations of the transmitter and reciever relative to the bedrock reflection surface. Figure 4B is a closeup of figure 4 indicating the slope correction necessary for measuring vertical ice thickness rather than distance from the transmitter to the nearest reflection surface (Kennard, 1983).

Correction for bedrock slope using measuring point migration

Initially, the basal altitude below each measured point was assumed to be the surface altitude less the apparent thickness (fig. 4A). However, because radar reflects off the nearest rock surface, a migration correction is required to find the true thickness vertically beneath each point.

The ice-depth equation (eq. 1) defines an ellipsoid, with the radar source and receiver at the respective foci. Theoretically, the reflection point could lie anywhere on this surface. If the measurements were taken within a distance of each other equal to an ice depth, a true reflection surface could be constructed by the envelope of the intersections of the various ellipsoids. In all but one instance, measurements were too far apart to allow construction of an envelope, and a geometrical migration scheme was required to determine the basal geometry.

For example, with a measurement made on steep ice in the middle of a glacier, the reflection point would most likely come from rock at an angle to the point and not directly below it (fig. 4B). Similarly, a sounding taken on a flat section of glacier near the valley wall would most likely be reflected from the side rather than from directly below. Because a map projection of the glacier was used, knowledge of the vertical distance between the measuring point and the bedrock (h') was required. This was calculated by:

$$h' = \frac{h}{\cos b}, \qquad (2)$$

where b was measured along the bedrock slope and through the measurement point.

For purposes of migration only, the above equation assumes the transmitted radio wave to be spherical, introducing negligible error for typical readings. Using the basal map developed with apparent thicknesses, angle b was computed by measuring the distance between contours along a curve perpendicular to the contours and passing through the measurement point.

Using this estimate of basal slope in the immediate measurement area, the apparent thickness was migrated, yielding an estimated base elevation directly below each measurement point. This was used to revise the basal contour map; a new basal slope was measured and the process repeated. This migration scheme was iterated, usually three or four times, with changes up to several millimeters at the map scale, until the base elevation value ceased changing. When drawing contours around individual measurement points, the estimated thickness was not expected to apply directly to the base area for more than approximately a distance equal to the ice thickness, though its influence on the contour pattern may have extended farther. If a contour were moved during migration, it was generally necessary to adjust the neighboring contours. Ice-surface features seen on aerial photographs were used as an aid in correctly locating the contours.

Use of maps and photographs to infer basal topography

The maps used were the most current Geological Survey topographic maps available for each area. The Mount Hood, Mount Shasta, and the Three Sisters maps were enlarged to a scale of 1:10,000, and the Mount Rainier map was used at the original scale of 1:24,000. Two hundred-foot contour intervals were used on Mount Rainier and to 100-foot intervals were used on the other mountains for ease in determining area and volume by altitude. Observations from photographs were an important part of map development, as they were useful as indicators of basal relief. Where available, some older photographs were examined showing lower ice levels and exposed basal relief (fig. 5A, 5B).

Field observations and autumn 1980 and 1981 aerial photographs were used to update the maps for current glacier boundaries, terminus positions, and perennial snow patch locations. Therefore, the resulting maps and values indicate areas and volumes in autumn, at the end of the ablation season.

Ice-Surface Features and their Relation to the Basal Topography

It is generally accepted that the surficial topography of a glacier reflects bed topography in diminished complexity, though bed features are reflected more accurately on the surface of thin ice than thick ice. It is possible through the judicious use of photographs to determine the trend of the basal topography for most glaciers.

Bedrock configurations induce flow regimes recognizable by characteristic crevasse patterns, but care must be taken when using these to infer basal topography. Interpretation of the crevasse patterns is necessary to distinguish between those caused by the shear stress along the valley walls, and those caused by local relief along the channel. Local changes in slope or channel width lead to areas of extending and compressing flow. Transverse crevasses tend to define areas of extending flow. In general, extending flow occurs above icefalls, and compressing flow occurs below them. Extending flow commonly occurs in accumulation areas. Crosshatched crevasse patterns may arise from ice flow over a bed bulge. A reduction of valley wall constraints often leads to splaying crevasses as seen near glacier termini. Generally, crevasses are products of stresses due to local topographic irregularities in the glacier bed, though they may move with the ice and from the area in which they formed.

Some surficial features bear no relation to bedrock topography. Wind-caused features and avalanche deposit zones can result in anomalous surface curvature. Convergent or divergent ice streams may deform the ice; these ice streams are detectable with their accompanying medial moraine, as seen during low-snow-year photography. Kinematic waves, in response to an accumulation perturbation may cause minor surface bulging independent of base morphology. Interpretation of photographs taken over several years allows identification of these phenomena.

Catastrophic events can have long-term effects on a glacier surface. Rock fall generally inhibits ice ablation, causing the underlying surface to appear raised, falsely indicating a bedrock rise. An example of this is at Lost Creek glacier on the South Sister (fig. 6), where existing maps show rockfall debris on the ice as bedrock, incorrectly indicating the glacier as two separate ice fields.

Figure 5A-5B--Two views across Nisqually Glacier toward Wilson Glacier illustrating the use of aerial photographs in determining the location of bedrock. Glacier conditions during 1944 permitted exposure of a bedrock cliff in lower Wilson Glacier seen near the center of the photograph; the same area with bedrock submerged during 1980. U.S. Geological Survey photographs by Fred Veatch on September 30, 1944 and by Carolyn Driedger on July 31, 1980.

Figure 6.--Rockfall partly concealing ice, as seen here on Lost Creek Glacier in the Three Sisters, must be identified as such for the proper volume estimation. U.S. Geological Survey photograph by Austin Post on September 10, 1980.

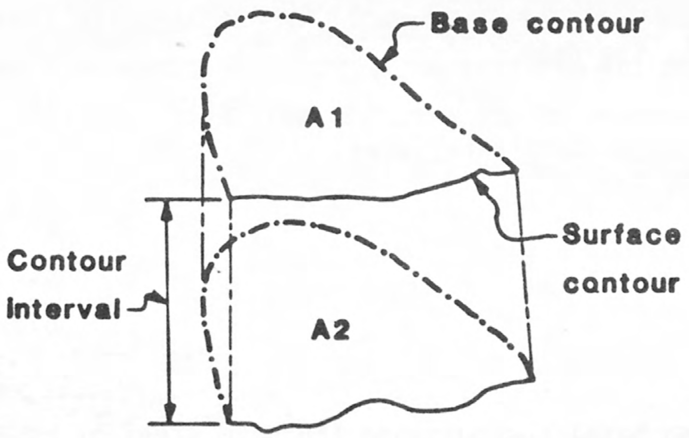

Figure 7.

Figure 7.--Sketch showing one volume element, which constructed over the length of the glacier permits calculation of volume on the measured glaciers. Each element consists of two horizontal planes (A1 and A2) which are formed by surface and basal contours separated by the contour interval (Kennard, 1983).

The end points of each basal contour to be drawn are known at the ice-rock boundary. From basal contours well constrained by radar measurements, it was seen that the exposed valley walls would maintain their configuration for a distance subglacially. This seemed particularly true where the valley wall was very steep in the lower reaches of a well-developed valley glacier. The presence of morainal debris and stream sediment at the glacier terminus was considered in this interpretation.

Despite the use of radar measurements and photographs, data were limited for defining small-scale features in the basal contours. This necessitated smoothing of the contours and the drawing of small-scale features only where strictly warranted by the data.

The primary component of the error is this extrapolation of the local bedrock depths over a large subglacial area. Error made in the interpretation of bedrock topography by use of radar measurements and photographs was calculated at 16 percent. This was calculated by using independent interpretations made by several glaciologists of ice depth of South Cascade Glacier, which has a volume well known from previous intensive radar measurements.

Isopach Maps as Interpretive Tools

Isopach maps (pls. 5, 6) are derived by the subtraction of altitudes between the surface and basal contours and indicate areas of equal ice thickness.

Although these values are defined explicitly by the surface-basal maps, the isopach contour connecting them is subject to interpretation. Again, the simplest solution was chosen, with curvature and number of areas bounded minimized. All radar points were checked to assure that they were located in the correct thickness field.

Analyses of isopach maps reveal patterns in the ice thickness that indicate ice falls, rock ribs, and basins or irregularities in the surface-based maps. Therefore, the isopach map became an interactive tool in the process of refining the basal contour maps. For all measured glaciers, a graph was prepared showing thickness as a function of area (figs. 11, 15, 19, 23).

DETERMINATION OF VOLUMES

Measured Glaciers

Glacier volumes were found by determining the area between each set of bedrock and surface contours, a pair of which define a volume element (fig. 7). Areas were measured with a planimeter or a digitizer to within 3 percent accuracy and were completed for the length of the glacier. Volumes (V) of each glacier were determined by using the volume-element areas in equation 3, where Ai is the area bounded by equal valued basal and surface contours at a given altitude and CI is the contour interval.

$$V = \frac{CI \sum_{i=1}^{n} \left[A_i + (A_{i+1}) \right]}{2} \qquad (3)$$

The contour interval used was 200 feet on Mount Rainier and 100 feet on Mounts Hood, Shasta, and the Three Sisters.

Glacier volumes were calculated by drainage area and altitude. Values for each drainage area, by mountain, are listed in tables 2 through 5. The percentage of the total ice and snow volume measured by radar varied for each mountain as follows: 62 percent on Mount Rainier, 83 percent on Mount Hood, 53 percent on the Three Sisters, and 19 percent on Mount Shasta.

The error in calculating volume varied with each glacier, depending on the number of measurement points per glacier. Error in snow patch and ice boundary corrections was estimated at 5 percent, and error from the original topographic maps was less than 5 percent. A conservative estimate for error in the volume of measured glaciers is $\pm$ 20 percent.

Unmeasured Glaciers and Snow Patches

Several different approaches have been made for estimating the volume or average thickness of unmeasured glaciers. For instance, Post and others (1971, p. 4) related average thickness to area size classes, using several measured glaciers for calibration. Kotliakov (1980) also incorporated the type of glacier in a similar scheme. Brückl (1973), Müller (1976, p. 12), Shih and others (1981, p. 194), Zhuravlev (1980), and Macheret and Zhuravlev (1982, p. 310) utilized an empirical relation of the form

$$\bar{h} = k_1 + k_2 A^m \tag{4}$$

where $\bar{h}$ is the mean glacier thickness, k_1, k_2, and m are coefficients derived from regression analysis, A is the glacier area, and $m \sim 0.5$.

Paterson (1970, p. 43) proposed that the shear stress on the bed be treated as a constant. For a simple, infinitely wide glacier with laminar flow, the shear stress on the bed τ is

$$\tau = \rho g h \sin \alpha \tag{5}$$

where ρ is the ice density, g the acceleration of gravity, h the ice thickness, and α the surface slope (Nye, 1952, p. 529). Thus, mean thickness can be calculated from the relation

$$\bar{h} = k_3/\alpha \tag{6}$$

where α is the surface slope and k_3 includes the assumed shear stress as well as ice density and geometric variables. However, none of these relations have been tested on glaciers of the type occurring on Cascade volcanoes.

Because glacier characteristics are related to latitude and climatic conditions, it was necessary to develop a volume estimation method for use in the Cascade Range. The volumes of unmeasured glaciers were estimated from statistical analysis of characteristics for all measured glaciers except the Whitney, which was examined during later study (Kennard, 1983). The variables required for these volume estimations can be determined from topographic maps and aerial photographs.

Table 1.--Table showing glacier lengths, mean glacier basal shear stresses calculated at 1,000-foot intervals, and assignment of a method which gives the closest correlation with its measured volume, where A indicates a closer correlation with area, and B indicates a closer correlation with basal shear stress.

Measured glacier	Correlation group	Basal shear stress, in bars	Map length of glacier measured in thousands of feet
Emmons	B	1.6	23.5
Winthrop	B	1.4	26.5
Tahoma	B	1.4	24.3
Carbon	B	1.3	31.9
Nisqually	B	1.4	21.7
Eliot	B	1.4	13.1
Wilson	B	1.2	8.5
Coe	B	1.3	10.7
Whitney	A	0.5	9.2
Russell	A	0.7	7.8
Newton Clark	A	0.5	6.7
Sandy	A	0.7	6.4
Collier	A	0.3	6.9
Prouty	A	0.5	5.1
Ladd	A	0.8	6.6
Reid	A	0.7	6.4
ZigZag	A	0.6	8.0
Hayden	A	0.6	4.3
Diller	A	0.5	3.9
White River	A	0.4	6.1
Lost Creek	A	0.4	4.7
Langille	A	0.6	4.8
Palmer	A	0.6	1.4
Coalman	A	0.6	1.6

Paterson's assumption of a constant basal shear stress, which is equivalent to the assumption that glacier flow can be treated by plasticity theory (Nye, 1951, p. 554), was tested by comparing shear stress (eq. 5) with other glacier characteristics. It was found that the larger glaciers had shear stress values in the expected range for glacier ($1<\tau<2$ bars). However, the smaller glaciers had lower values of shear stress, ranging down almost to zero.

It would appear that some glaciers reach a critical basal shear stress, and for these glaciers, the flow is sufficiently fast to adjust the longitudinal profile to a dynamic equilibrium so that the product of thickness and surface slope is related to that stress. Other glaciers are too small to reach that critical shear stress, and their profiles are determined less by dynamic considerations than by local variations in snow drifting and melting. In an analysis of the measured glaciers (table 2), it was found that most glaciers having a length greater than 8,500 ft obtained a critical shear stress, and most glaciers with lengths less than this did not. It was also found that an estimated basal shear stress τ^* in pounds per square foot for the larger glaciers could be calculated by the empirical relation

$$\tau^* = 451.12\left(\sum \frac{A_i}{\cos \alpha_i}\right)^{.106}, \tag{7}$$

where ΣA_i in feet squared is the sum of surface area at 1,000-foot altitude intervals. Noting that volume $V = Ah$, the estimated volume V^* in cubic feet can be calculated using the estimated shear stress τ^* according to

$$V^* = \tau^*/[\rho g \sum(A_i/(\cos\alpha_i)\ (\sin\alpha_i))], \tag{8}$$

where area and slope were measured at 1,000-foot intervals and then summed.

The volume of small glaciers, those that do not obtain the critical shear stress, were generally those less than 8,500 ft in length (Kennard, 1983). The empirical relationship is

$$V = 9.62A^{1.124}, \tag{9}$$

where V = volume in cubic feet of the total glacier, and A = total area in square feet. The Whitney glacier on Mount Shasta, though measured by ice radar, is on the border of having a closer area correlation than a basal shear stress correlation. Its length is 9,200 ft but its shear stress is only 0.9 bars. Perhaps this may be explained by the presence of a substantial icefall around 11,800 ft which interrupts the normal glacier flow, essentially making it into two smaller glaciers. Some glaciers do not occupy discrete valley basins and their bedrock topography divides the glacier area into separate units. These should be treated separately for area determination and the results should be summed. Therefore, an experienced eye and much discretion are required in the application of and selection of a method for determining ice volume.

When the estimation methods were developed they were tested by application to glaciers with measured volumes. The standard deviations of errors of estimated and measured volumes were as follows: 5 percent for large glaciers (with

Table 2.--Areas and volumes of glacier ice and snow on Mount Rainier. Methods of determination = M, glacier thickness measured by ice radar; B, volume estimated with calculation of basal shear stress; A, volume estimated using area correlation.

		Altitude Interval										
		3,000-6,000'		6,000-9,000'		9,000-12,000'		12,000-14,410'				
Drainage area	Glacier or snow patch	Area (ft^2) [x 10^6]	Volume (ft^3) [x 10^9]	Area (ft^2) [x 10^6]	Volume (ft^3) [x 10^6]	Area (ft^2) [x 10^6]	Volume (ft^3) [x 10^9]	Area (ft^2) [x 10^6]	Volume (ft^3) [x 10^9]	Area total (ft^2) [x 10^6]	Volume total (ft^3) [x 10^9]	Method of determination
Cowlitz River	Snow patch	2.5	--	11.	--	.5	--	.02	--	14.0	.7	B
	Whitman	--	--	19.0	--	4.8	--	--	--	23.8	4.4	A
	Ingraham	3.56	--	18.8	--	16.6	--	3.6	--	42.6	7.0	A
	Cowlitz	4.5	--	21.3	--	11.0	--	--	--	36.8	6.0	A
	Paradise	--	--	10.9	--	--	--	--	--	10.9	.8	B
	Ohana-pecosh	.3	--	17.0	--	--	--	--	--	17.3	1.3	B
	Subtotal	10.9	--	98.0	--	32.9	--	3.6	--	145.4	20.2	--
Nisqually River	Snow patches	--	--	7.4	--	.5	--	.4	--	8.3	.3	B
	Muir Snowfield	--	--	2.8	--	7.3	--	--	--	10.1	.7	B
	Nisqually	5.7	1.4	20.	3.5	12.4	1.4	11.6	1.5	49.7	7.8	M
	Wilson	--	--	10.8	1.6	4.7	.3	--	--	15.5	1.9	M
	Kautz	--	--	6.4	--	5.7	--	.3	--	12.4	1.3	B
	Success	--	--	3.6	--	3.8	--	--	--	7.4	.5	B
	Van Trump	--	--	5.6	--	1.1	--	--	--	6.7	.5	B
	Pyramid	--	--	5.6	--	.2	--	--	--	5.8	.4	B
	S. Tahoma	2.6	--	19.5	--	8.1	--	.2	--	30.4	4.6	A
	Tahoma	3.6	.4	18.2	2.9	5.0	.5	5.3	.5	32.1	4.3	M
	Subtotals	11.9		99.9		48.8		17.8	--	178.4	22.3	--

Table 2.--Mount Rainier areas and volumes (continued).

Drainage area	Glacier or snow patch	Altitude Interval: 3,000-6,000' Area (ft^2) [x 10^6]	3,000-6,000' Volume (ft^3) [x 10^9]	6,000-9,000' Area (ft^2) [x 10^6]	6,000-9,000' Volume (ft^3) [x 10^6]	9,000-12,000' Area (ft^2) [x 10^6]	9,000-12,000' Volume (ft^3) [x 10^9]	12,000-14,410' Area (ft^2) [x 10^6]	12,000-14,410' Volume (ft^3) [x 10^9]	Area total (ft^2) [x 10^6]	Volume total (ft^3) [x 10^9]	Method of determination
Puyallup River	Snow patch	--	--	9.7	--	.2	--	--	--	9.9	.4	B
	Tahoma	5.1	1.0	23.0	5.6	18.8	2.7	13.96	2.5	60.8	11.8	M
	N Mowich	3.0	--	48.3	--	13.7	--	1.4	--	66.4	9.5	A
	Liberty Cap	--	--	--	--	.4	--	1.3	--	1.7	.1	A
	Flett	--	--	3.2	--	--	--	--	--	3.2	.2	B
	Edmonds	--	--	11.3	--	3.7	--	--	--	15.0	1.1	B
	S Mowich	.8	--	16.4	--	19.5	--	1.7	--	38.4	4.5	A, B
	Puyallup	1.1	--	38.2	--	13.6	--	1.9	--	54.8	10.2	A
	Subtotals	10.0	--	150.1	--	69.9	--	20.2	--	250.2	37.8	--
Carbon River	Snow patch	.3	--	9.2	--	--	--	--	--	9.5	.5	B
	Carbon	26.6	11.4	46.1	12.6	9.4	.8	3.1	.2	85.2	25.1	M
	Russell	--	--	33.2	3.0	2.3	.1	--	--	35.5	3.1	M
	Subtotals	26.9	--	88.5	--	11.7	--	3.1	--	130.2	28.7	--
White River	Snow patch	.9	--	16.6	--	1.1	--	--	--	18.6	1.0	B
	Winthrop	18.5	3.6	44.3	9.7	23.7	3.4	11.6	1.8	98.1	18.5	M
	Emmons	16.4	6.1	55.7	11.8	39.4	4.9	8.7	.9	120.2	23.8	M
	Inter	--	--	7.4	--	1.0	--	--	--	8.4	.6	B
	Frying Pan	32.4	--	2.8	--	--	--	--	--	35.2	2.9	B.
	Sarvant	.1	--	6.1	--	--	--	--	--	6.2	.4	B
	Subtotals	68.3	--	132.9	--	65.2	--	20.3	--	286.7	47.2	--
Area Total		128.0		569.4		228.5		65.0		991.0		
Volume Total											155.8	

volumes found using equations 6 and 7), 16 percent for small glaciers (using equation 8), and 13 percent for the groups together. Together with a ± 20 percent uncertainty in finding measured glacier volumes, the error in using the estimation method is assumed to be about ± 25 percent.

Both estimation methods yield volume by total glacier area and not by altitude interval. As total glacier areas are required for computing glacier volumes, areas can not be split by percent to obtain corresponding altitude interval volumes without introducing additional significant error. Therefore, where area and volume are listed by elevation in tables 2, 3, 4, and 5, volume is listed for measured glaciers only.

RESULTS: FOUR CASCADE VOLCANOES

Mount Rainier

Mount Rainier is west of the Cascade crest about 40 miles southeast of Tacoma Wash. (fig. 8). The mountain, rising to 14,410 ft above sea level, dominates the landscape, and in fact, its geologic development has affected much of the surrounding local topography.

Water flows from the mountain in five major drainage basins. The Nisqually, Puyallup, Carbon, and White Rivers flow into Puget Sound, and the Cowlitz River flows into the Columbia River. Figure 9 indicates that the largest areas of snow and ice cover are in the watersheds of the Puyallup River (twenty-five percent) and the White River (twenty-nine percent).

There are presently 23 major glaciers on Mount Rainier. These glaciers are some of the most accessible to the public in the nation. Descriptions and research on some, such as the Nisqually Glacier, date back to 1870 (Heliker and others, 1983, p. 3).

The five glacier systems measured on Mount Rainier are the Nisqually-Wilson, Tahoma, Carbon-Russell, Winthrop, and the Emmons. The volume of ice and snow on Mount Rainier is 155.8 billion ft^3. Glacier and snowpatch dimensions are listed by drainage area and by altitude in table 2. The maximum ice thickness measured on Mount Rainier is 705 ft, in the Carbon Glacier. With a volume of 25.1 billion ft^3, the Carbon Glacier has the largest volume of the Rainier glaciers. At 3,500 ft in altitude, its terminus is the lowest of any in the counterminous States. The Nisqually Glacier, a glacier more commonly viewed by the public, has a surface area of 49.7 million ft^2, whereas the Emmons has the largest surface area, at 120.2 million ft^2. Figures 9 and 10 show ice volumes for radar-measured glaciers, and ice areas by drainage as a function of altitude. Figures 11 A-F show measured ice areas at the indicated thickness intervals. Plate 1 is a map showing 1981 snow and ice boundaries and basal contours for the measured glaciers. Plate 2 shows the isopach maps derived from the surface-basal mapping of measured glaciers.

The interaction between glacial and volcanic activity predates the existing volcano form. Glacial till estimated to be as much as 600,000 years B.P. is covered by more recent intracanyon lava flows (Crandell and Miller, 1974, p. 17). More recently, the melting of ice and snow has in part been responsible for mudflows which extended to Enumclaw 6,000 years B.P. and to Orting about 500 years B.P. (Crandell and Mullineaux, 1981, p. 14). Figure 9 illustrates that fifty percent of snow and ice on the mountain between altitudes of 6,000 and 9,000 feet; thirty percent is above 9,000 feet.

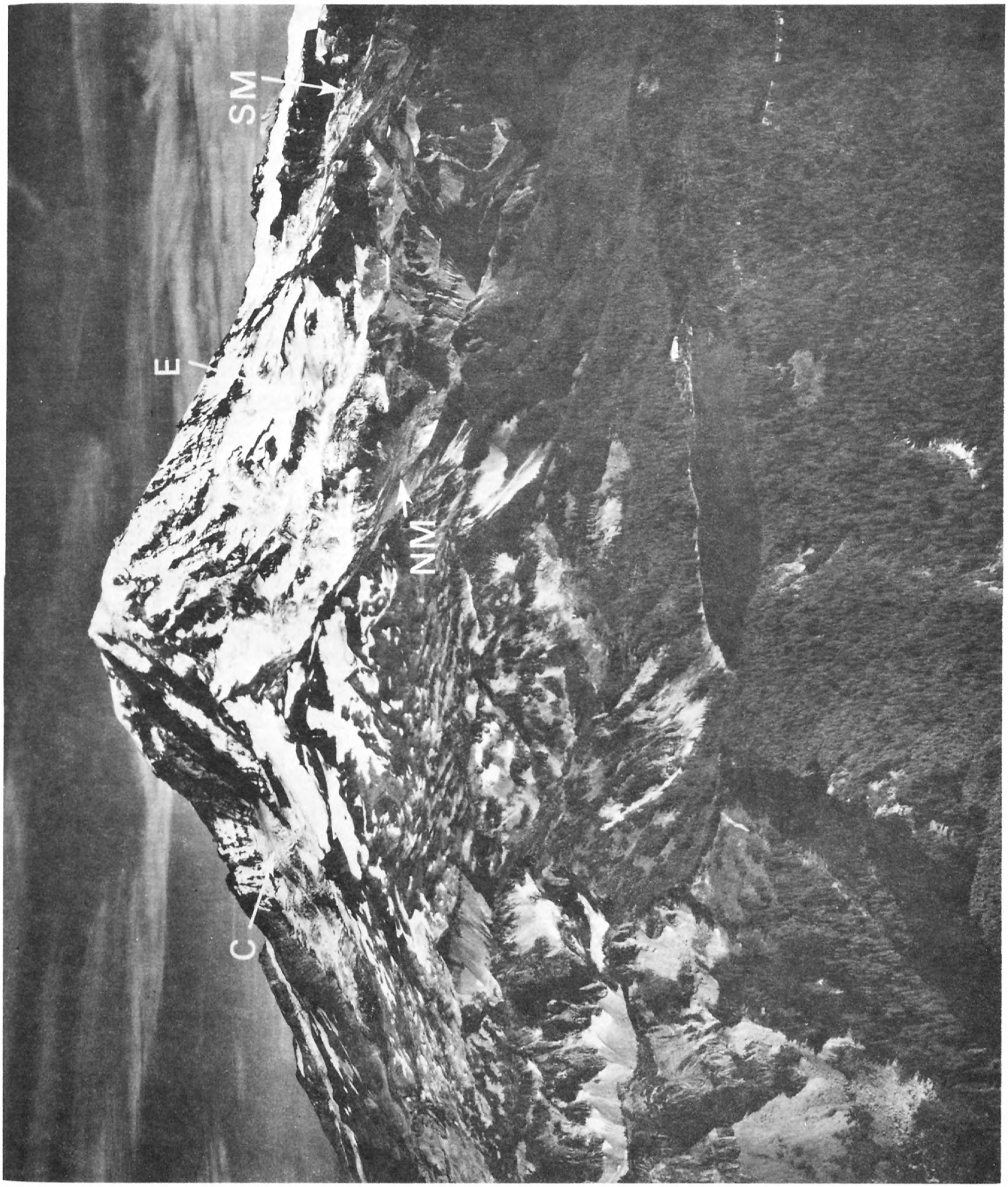

Figure 8.--Mount Rainier as seen from the northwest, showing the C, Carbon; NM, North Mowich; E, Edmunds; and SM, South Mowich glaciers. Mowich Lake is in the foreground. U.S. Geological Survey photograph by Robert Krimmel on August 17, 1981.

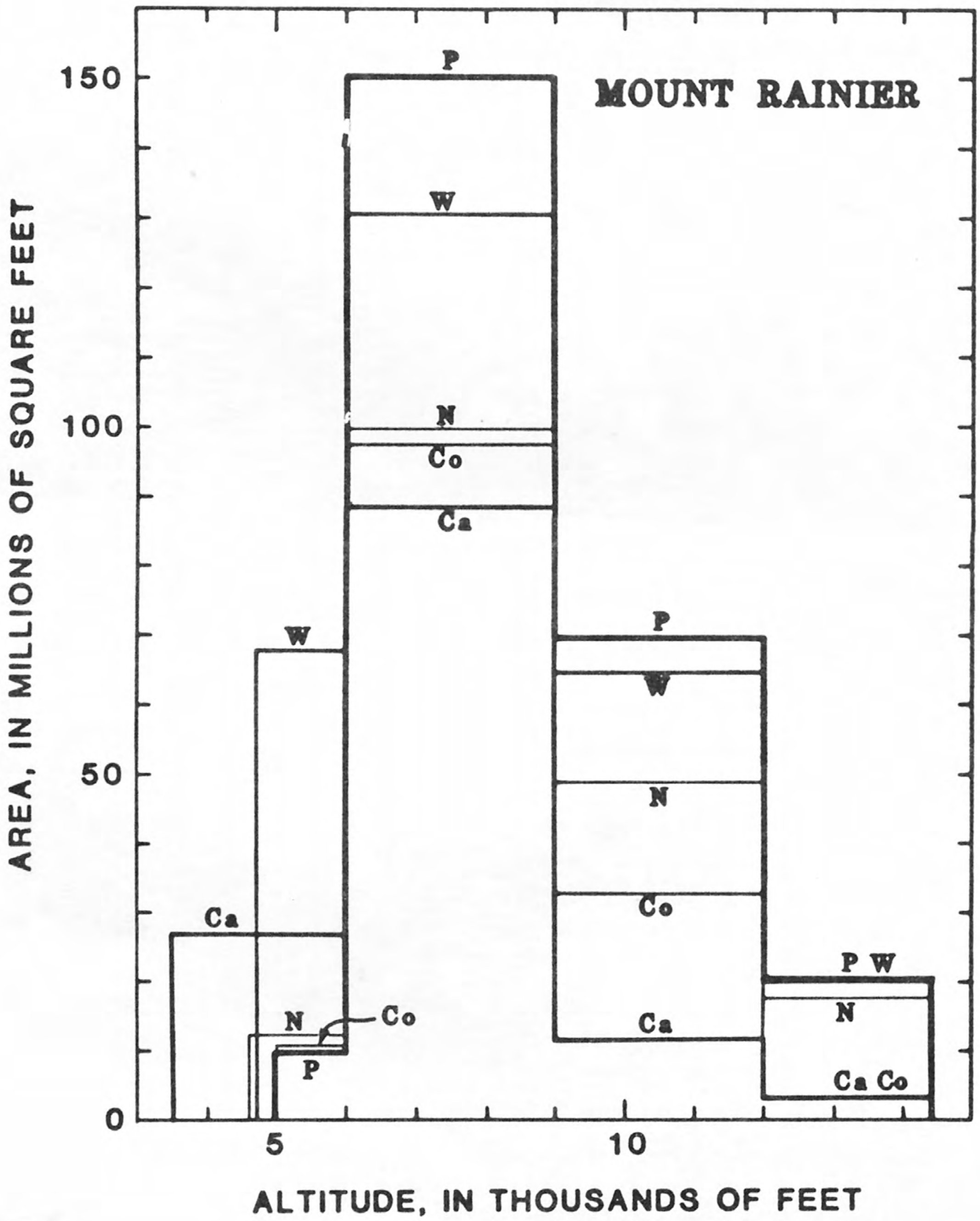

Figure 9.

Figure 9.--Areas of ice and snow in Mount Rainier glacier drainage basins as a function of altitude. Drainage basins listed are as follows: Ca, Carbon; W, White River; Co, Cowlitz; N, Nisqually; P, Puyallup.

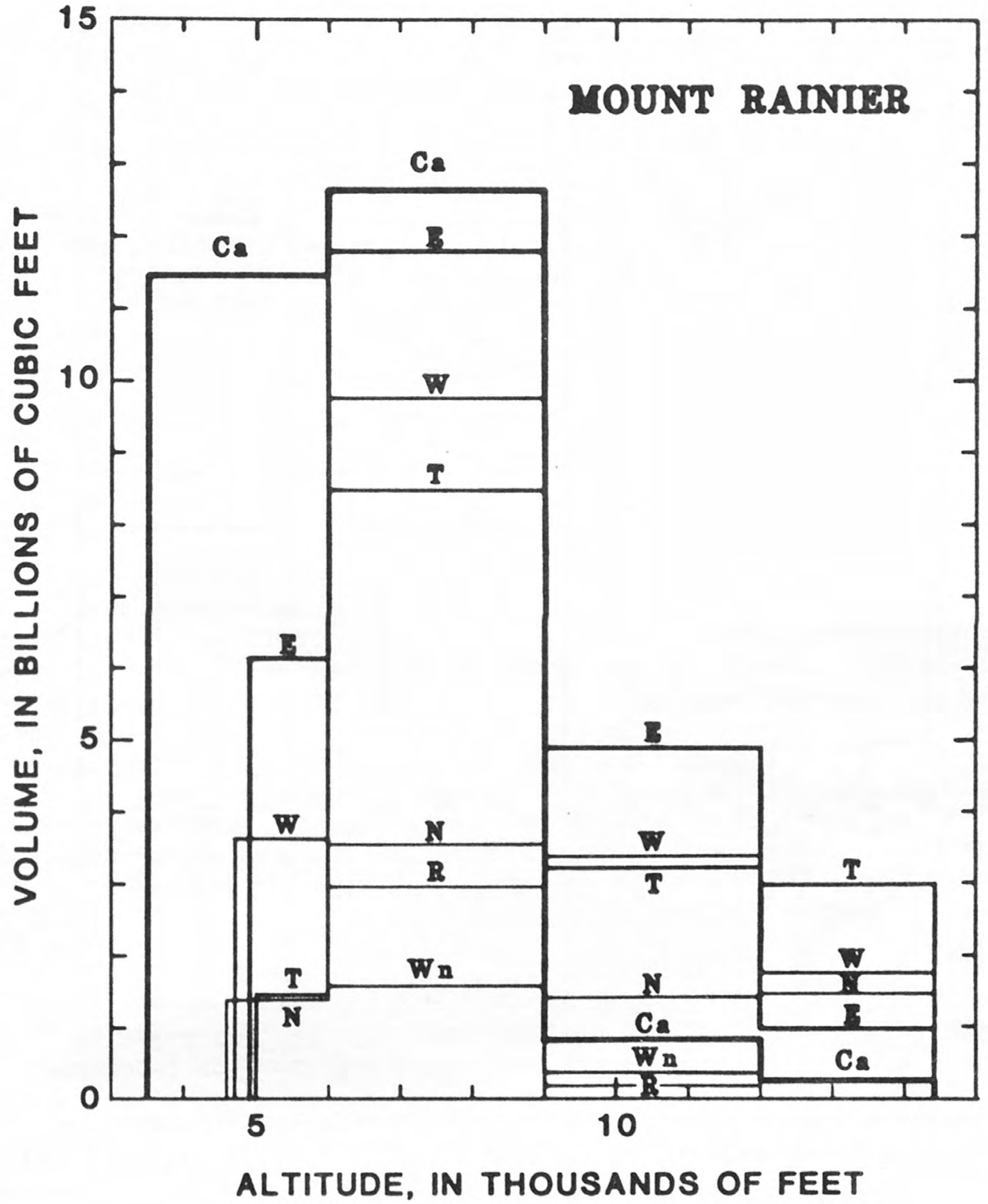

Figure 10.

Figure 10.--Ice volume of measured Mount Rainier glaciers as a function of altitude. Glaciers listed are as follows: Ca, Carbon; E, Emmons; N, Nisqually; T, Tahoma; W, Winthrop; Wn, Wilson; R, Russell.

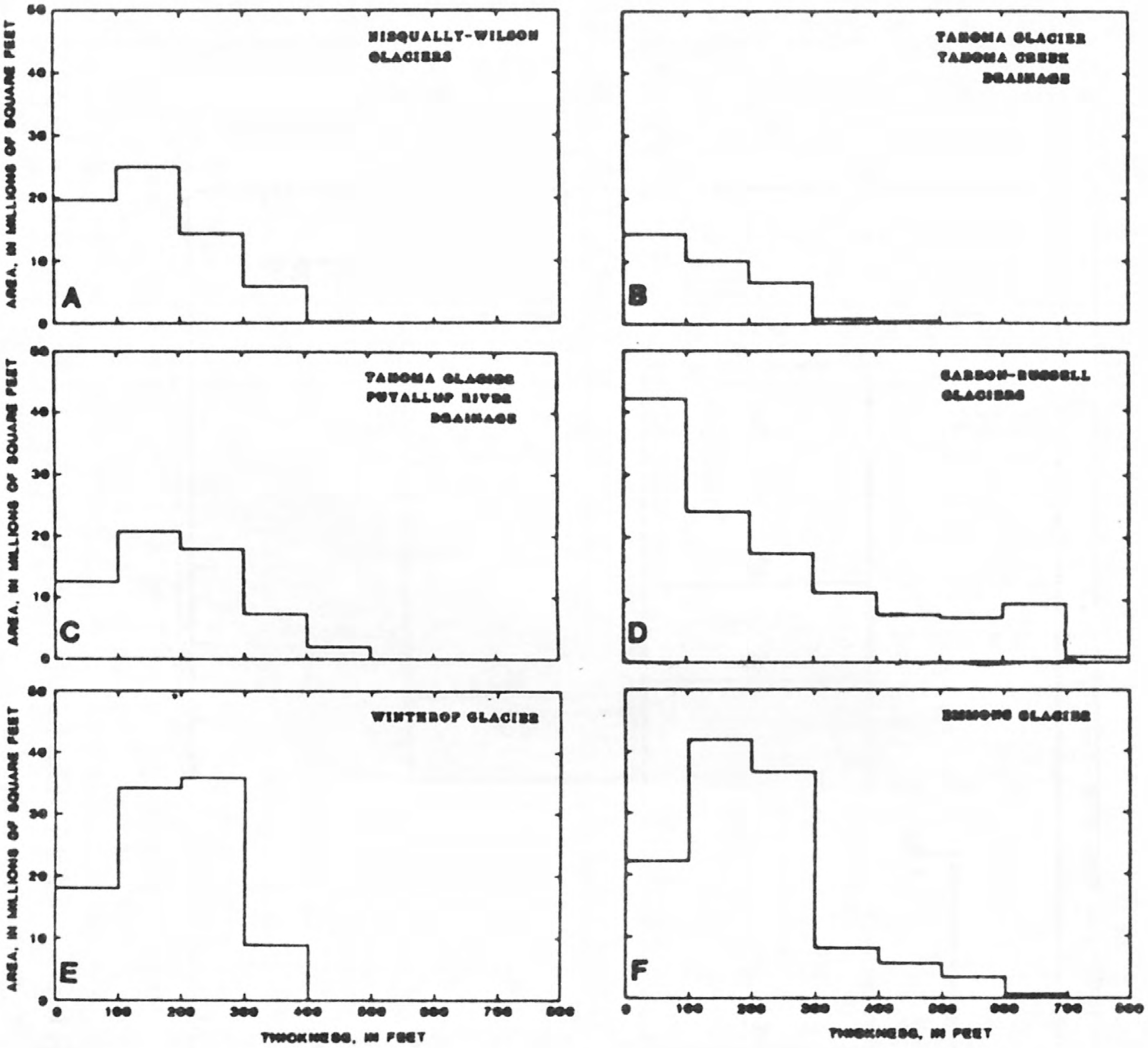

Figure 11

Figures 11A-F.--Areas of selected thickness intervals of radar-measured glaciers of Mount Rainier. Values are derived from isopach maps.

Lahars are mudflows and debris flows of volcanic material derived from the slope of a volcano and sometimes mobilized with melting snow and ice. They occur most often during periods of eruption, and, at Mount Rainier, they have occurred most frequently during historic times in the valleys of the White, Nisqually, and Mowich Rivers, and Tahoma and Kautz Creeks. Lahars from Mount Rainier constititute the major threat to people and property during volcanic eruptions (Crandell, 1971, p. 69).

The area on Mount Rainier above 12,000 ft is approximately the region of the old summit depression containing two craters and has an ice volume of 8.7 billion ft^3. The principal eastern crater tilts toward the east, indicating that this may be the first direction that meltwater in the center might flow. In such a situation, the Cowlitz, Ingraham, Emmons, and Winthrop glaciers would be most affected, possibly causing lahars and floods in the valleys of the Cowlitz and White Rivers. The volumes of ice and snow are 20.2 billion ft^3 in the Cowlitz River and 47.2 billion ft^3 in the White River drainage areas. Further descriptions of Mount Rainier eruptive hazards are found in a publication by Crandell and Mullineaux (1981).

Mount Hood

Mount Hood rises to 11,245 ft and is approximately 50 miles east of Portland, Oreg. (fig. 12). All the Mount Hood drainage streams, (White, Zig Zag, Sandy, and Hood Rivers) empty into the Columbia River. Figure 13 illustrates that sixty percent of the total are covered by snow and ice is in the Hood watershed.

Ice-volume measurements were made on all nine major glaciers of Mount Hood. The total volume of ice and snow on Mount Hood is 12.2 billion ft^3. Glacier and snowpatch dimensions are listed by drainage area and by elevation in table 3. The Eliot Glacier has the largest volume, 3.2 billion ft^3, and thickest measured ice, 361 ft. The Coe-Ladd Glacier system has the largest surface area, 23.1 million ft^2.

The ice and snow boundaries on Mount Hood and basal contours for the measured glaciers in 1981 are shown on plate 3. The isopach maps derived from the surface-basal contours are shown on plate 5.

Mount Hood's composite cone was built during late Pleistocene time (Wise, 1969, p. 969). It's earliest known major eruptive period after the glacial maximum occurred 12,000 to 15,000 years B.P., which, along with two other major eruptive periods (1,500-1,800 and 200-300 years B.P.) produced much of the mountain visible today (Crandell, 1980, p. 1). Much of the topography on the lower slopes of Mount Hood is the result of mudflows and pyroclastic flows, which were formed during the Polallie eruptive period of 12,000 to 15,000 years B.P., and may have been aided by eruption-related icemelt. The absence of these deposits in some valleys indicates the extent of former glaciers (Crandell, 1980, p. 11).

As on Mount Rainier, the river valleys radiating from Mount Hood contain valuable timber and recreational property. The geologically recent eruptive history and hazards of Mount Hood were more comprehensively described in Crandell (1980).

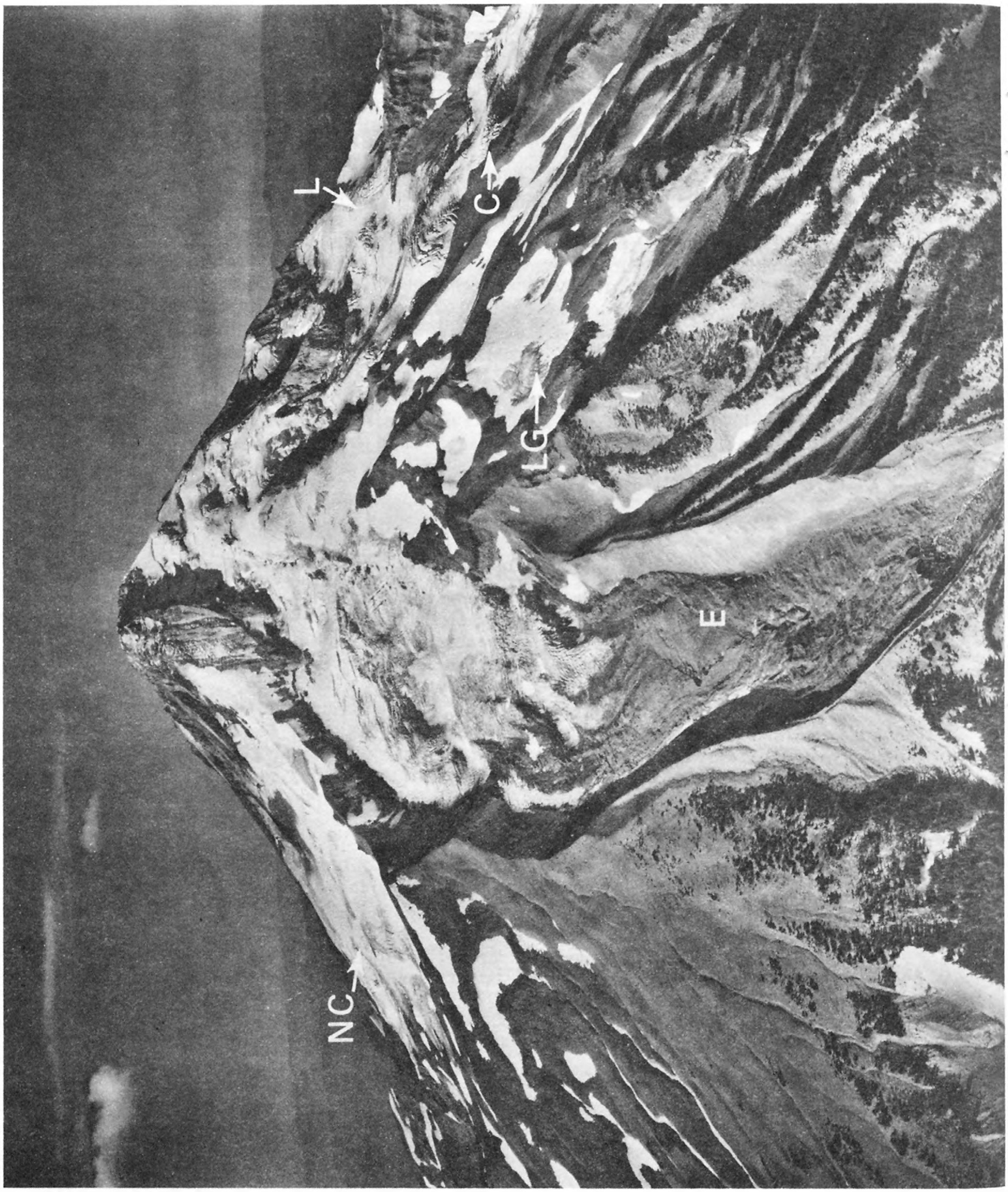

Figure 12.--Mount Hood, Oregon, as seen from the east, showing (left to right) N, Newton Clark; E, Eliot; LG, Langille; C, Coe; and L, Ladd Glaciers. U.S. Geological Survey photograph by Austin Post on September 10, 1980.

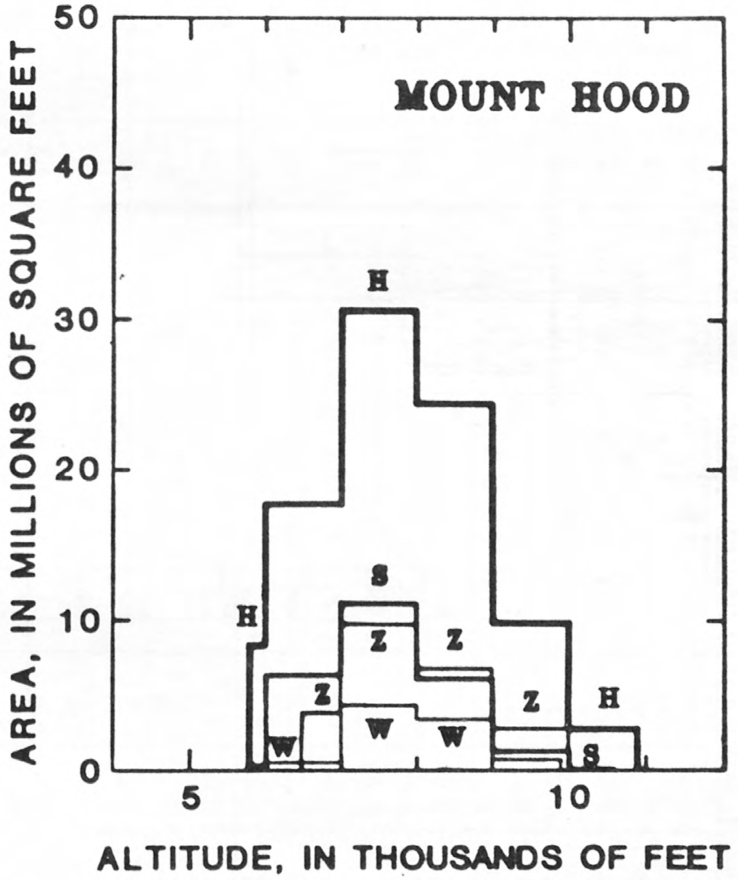

Figure 13.

Figure 13.--Areas of ice and snow in Mount Hood glacier drainage basins as a function of altitude. Drainage basins listed are as follows: H, Hood River; S, Sandy River; W, White River; Z, Zig Zag.

Table 3.--Areas and volumes of glacier ice and snow on Mount Hood. Methods of determination = M, glacier thickness measured by ice radar; B, volume estimated with calculation of basal shear stress; A, volume estimated using area correlation.

Drainage area	Glacier or snow patch	Altitude Interval														Area total (ft^2) [x 10^6]	Volume total (ft^3) [x 10^9]	Method of determination
		5,000-6,000'		6,000-7,000'		7,000-8,000'		8,000-9,000'		9,000-10,000'		10,000-11,000		11,000-Summit				
		Area (ft^2) [x 10^6]	Volume (ft^3) [x 10^9]	Area (ft^2) [x 10^6]	Volume (ft^3) [x 10^6]	Area (ft^2) [x 10^6]	Volume (ft^3) [x 10^9]	Area (ft^2) [x 10^6]	Volume (ft^3) [x 10^9]	Area (ft^2) [x 10^6]	Volume (ft^3) [x 10^9]	Area (ft^2) [x 10^6]	Volume (ft^3) [x 10^9]	Area (ft^2) [x 10^6]	Volume (ft^3) [x 10^9]			
White River	Snow patches	--	--	.5	--	1.2	--	.8	--	.4	--	--	--	--	--	2.9	.2	B
	Coalman	--	--	--	--	--	--	--	--	--	--	.6	.03	--	--	.6	.03	M
	White River	--	--	.01	.0008	3.2	.2	2.3	.19	.3	.008	--	--	--	--	5.8	.3	M
	Subtotal	--	--	.5	--	4.4	--	3.1	--	.7	--	.6	--	--	--	9.3	.5	--
Hood River	Snow patches	.5	--	8.3	--	9.9	--	.6	--	--	--	--	--	.1	--	19.4	1.0	B
	Newton-Clark	--	--	--	--	2.1	.05	12.3	.9	5.7	.4	1.3	.03	--	--	21.4	1.4	M
	Coe	.3	.09	3.7	.5	5.0	.8	2.0	.2	1.7	.2	.7	.04	--	--	13.4	1.9	M
	Ladd	--	--	1.0	.04	5.9	.5	2.5	.3	.3	.01	--	--	--	--	9.7	.9	M
	Eliot	--	--	4.6	.9	7.2	1.4	4.1	.7	1.3	.1	.9	.1	--	--	18.1	3.2	M
	Langille	--	--	--	--	.4	.02	2.9	.2	1.0	.06	--	--	--	--	4.3	.3	M
	Subtotal	.8	--	17.6	--	30.5	--	24.4	--	10.0	--	2.9	--	.1	--	86.3	8.7	--
Zig Zag River	Snow patches	--	--	3.9	--	7.8	--	1.5	--	.5	--	--	--	.2	--	13.9	.7	B
	Zig Zag	--	--	--	--	1.3	.04	4.5	.3	2.4	.2	.1	.005	--	--	8.3	.6	M
	Palmer	--	--	--	--	.6	.04	.8	.03	--	--	--	--	--	--	1.4	.07	M
	Coalman	--	--	--	--	--	--	--	--	--	--	.3	.01	--	--	.3	.01	M
	Subtotal	--	--	3.9	--	9.7	--	6.8	--	2.9	--	.4	--	.2	--	23.9	1.4	--
Sandy River	Snow patches	.2	--	2.3	--	.8	--	.4	--	.3	--	.6	--	.1	--	4.7	.2	B
	Sandy	--	--	3.1	.1	8.0	.6	1.7	.1	--	--	--	--	--	--	12.8	.8	B M
	Reid	--	--	.9	.03	2.2	.1	4.0	.4	1.0	.06	--	--	--	--	8.1	.6	M
	Subtotal	.2	--	6.3	--	11.0	--	6.1	--	1.3	--	.6	--	.1	--	25.6	1.7	--
Area Total		1.0		28.3		55.6		40.4		14.9		4.5		.4		145.1		
Volume Total																	12.2	

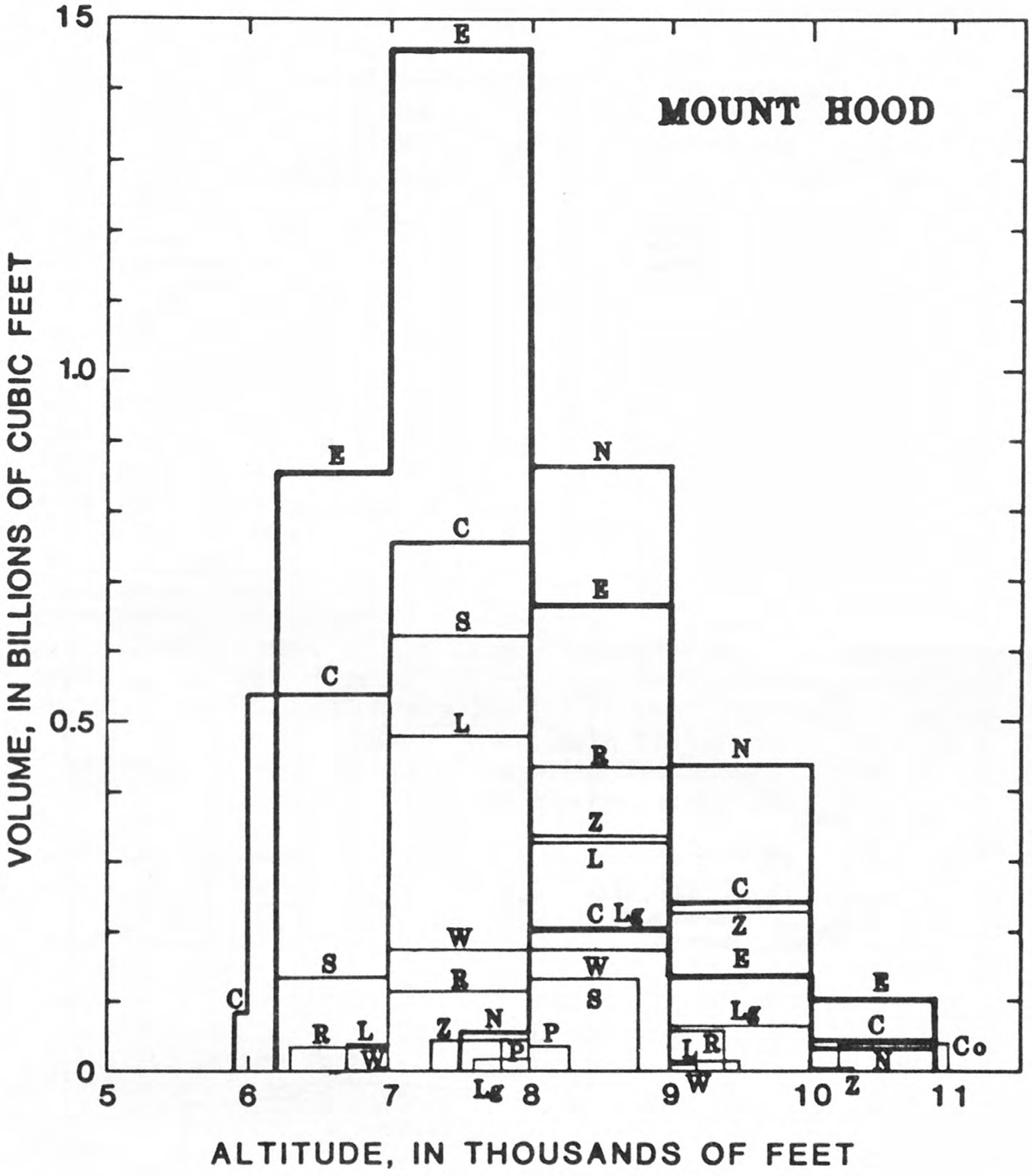

Figure 14.

Figure 14.--Ice volume of measured Mount Hood glaciers as a function of altitude. Glaciers listed are as follows: C, Coe; Co, Coalman; E, Eliot; L, Ladd; La, Langille; N, Newton Clark; P, Palmer; R, Reid; S, Sandy; W, White River; Z, Zig Zag.

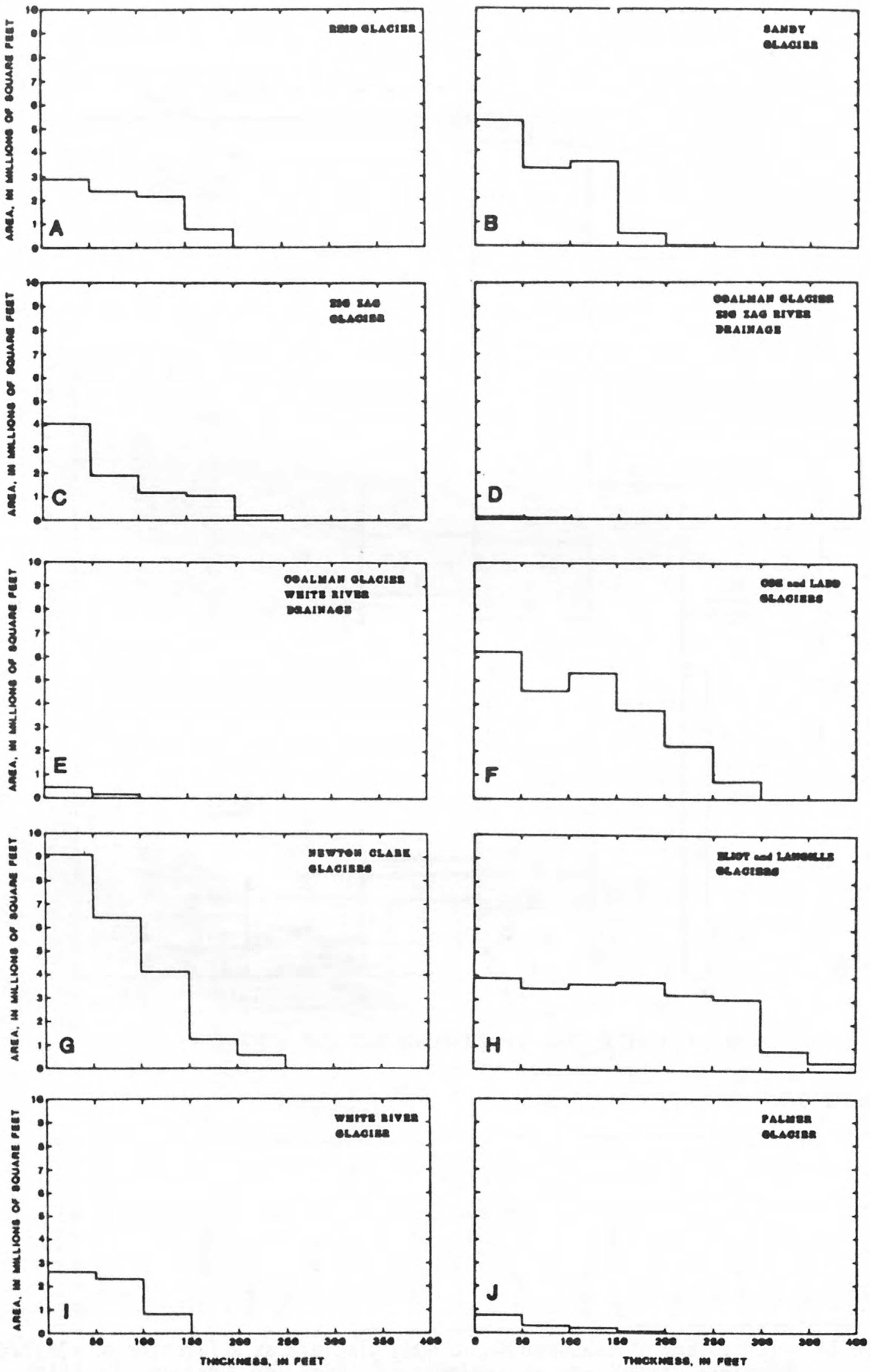

Figures 15A-J.--Areas of ice for each thickness interval of radar-measured glaciers. Values are derived from isopach maps of Mount Hood (Kennard, 1983).

At Mount Hood flooding and lahars are the principal eruptive hazard to these resources. Crandell (1980, p. 56) stated that they represent a hazard in the valleys--up to several tens of feet high on the valley walls and higher where the valley is constricted. Interpretations of the hazard map developed by Crandell, indicate that a dome-building eruption in the present Crater Rock region might deposit debris on the White River, Palmer, Zig Zag, and Reid Glaciers, and affect about 2 billion ft^3 of ice and snow. The volume of ice above 10,000 ft in the vicinity of Crater Rock is about 47 million ft^3. About eighty percent of the total area of snow and ice cover is above 7,000 feet in altitude.

An eruption outside the debris fan region, but near the summit, might cause eruptive deposits on the remainder of the Mount Hood glaciers, which have an ice and snow volume of 10.5 million ft^3.

Three Sisters

In this report, the Three Sisters collectively refer to the North Sister, Middle Sister and South Sister, three volcanic cones located in an extensive volcanic region about 30 miles west of Bend, Oreg. The Three Sisters have a total ice and snow volume of 5.6 billion ft^3, as seen in table 4.

Four major streams drain the Three Sisters. Separation Creek and White Branch drain the west sides of the mountains and empty into the McKenzie River. Squaw Creek drains most of the Three Sisters' east side and empties into the Deschutes River, after flowing through the town of Sisters. Forty-three percent of the total surface area of snow and ice is in the Squaw Creek watershed. Fall Creek drains the southeastern part of South Sister, where flank eruptions have occurred in postglacial time. Five miles from South Sister it empties into Sparks Lake, which has no surface outlet.

Radar measurements were made on the five major glaciers on the Three Sisters: Hayden, Diller, Collier, Prouty, and Lost Creek Glaciers. As seen in table 3, Collier Glacier is the largest, with a surface area of 11.8 million ft^2, a volume of 0.7 million ft^3, and the greatest ice thickness at 300 ft. Plate 4 displays basal contours and plate 5 displays isopachs for the measured glaciers.

Volcanism in the Three Sisters region is varied in origin and type, with eruptions predating and postdating the eruption of Mount Mazama about 6,800 years B.P. (Wozniak and Taylor, 1981, p. 61). The larger relief features consist of three cones more than 10,000 ft in altitude- North, Middle, and South Sisters, which erupted in pre-Holocene time--and the smaller cones of Broken Top (pre-Holocene) and Bachelor Butte (Pleistocene to Holocene time, fig. 16). More recently, basalt has flowed over extensive regions north and south of the Three Sisters. A rhyodacitic flank eruption on the south side of South Sister is the most recent activity on the Sisters cones.

The lack of widespread mudflow and pyroclastic deposits from the most recent summit eruptions on South Sister indicate that these eruptions may have occurred during late Wisconsin time when an extensive ice cover surrounded the cone. Though no direct geologic evidence exists to indicate large-scale glacier melting during past eruptions, there is evidence that some late Holocene flank eruptions were accompanied by small lahars, which were probably aided by rapid snowmelt (W. E. Scott, U.S. Geological Survey, written commun., May 18, 1983).

Table 4.--Areas and volumes of glacier ice and snow on Three Sisters. Methods of determination = M, glacier thickness measured by ice radar; B, volume estimated with calculation of basal shear stress; A, volume estimated using area correlation.

Drainage area	Glacier or snow patch	Altitude Interval										Area total (ft^2) [x 10^6]	Volume total (ft^3) [x 10^9]	Method of deter-mination
		6,000-7,000'		7,000-8,000'		8,000-9,000'		9,000-10,000'		13,000-14,162'				
		Area (ft^2) [x 10^6]	Volume (ft^3) [x 10^9]	Area (ft^2) [x 10^6]	Volume (ft^3) [x 10^6]	Area (ft^2) [x 10^6]	Volume (ft^3) [x 10^9]	Area (ft^3) [x 10^6]	Volume (ft^2) [x 10^9]	Area (ft^2) [x 10^6]	Volume (ft^3) [x 10^9]			
Squaw Creek	Snow patches	.1	--	4.7	--	1.5	--	.1	--	--	--	6.4	.3	B
	Linn	--	--	--	--	.6	--	--	--	--	--	.6	.03	B
	Villard	--	--	--	--	.1	--	.4	--	--	--	.5	.02	B
	Thayer	--	--	1.1	--	.6	--	--	--	--	--	1.7	.1	B
	Hayden	--	--	.7	.07	6.8	.6	.3	.009	--	--	7.8	.6	M
	Diller	--	--	2.9	.2	4.2	.3	--	--	--	--	7.1	.5	M
	Carver	--	--	1.9	--	1.6	--	--	--	--	--	3.5	.2	B
	Prouty	--	--	.3	.03	7.9	.4	2.3	.1	.004	.001	10.5	.7	M
	Collier	--	--	--	--	.4	.004	--	--	--	--	.4	.004	M
	Subtotal	.1	--	11.6	--	23.7	--	3.1	--	.004	--	38.5	2.5	--
Fall Creek	Snow patches	--	--	1.3	--	1.4	--	.4	--	--	--	3.1	.1	B
	Lewis	--	--	--	--	1.6	--	2.6	--	--	--	4.2	.3	B
	Subtotal	--	--	1.3	--	3.0	--	3.0	--	--	--	7.3	.4	--
Separ-ation Creek	Snow patches	--	--	.6	--	1.5	--	.6	--	--	--	2.7	.1	B
	Clark	--	--	--	--	3.0	--	--	--	--	--	3.0	.2	B
	Lost Creek	--	--	1.5	.05	4.1	.4	.2	.003	--	--	5.8	.4	M
	Crater	--	--	--	--	--	--	--	--	1.1	.07	1.1	.06	M
	Eugene	--	--	--	--	--	--	1.0	.006	--	--	1.0	.05	B
	Skinner	--	--	1.7	--	1.4	--	--	--	--	--	3.1	.2	B
	Irving	--	--	3.4	--	.6	--	.1	--	--	--	4.1	.3	B
	Subtotal	--	--	7.2	--	10.6	--	1.9	--	1.1	--	20.8	1.3	--

Table 4.--Three Sisters areas and volumes (continued).

Drainage area	Glacier or snow patch	Altitude Interval 6,000-7,000' Area (ft^2) [x 10^6]	6,000-7,000' Volume (ft^3) [x 10^9]	7,000-8,000' Area (ft^2) [x 10^6]	7,000-8,000' Volume (ft^3) [x 10^6]	8,000-9,000' Area (ft^2) [x 10^6]	8,000-9,000' Volume (ft^3) [x 10^9]	9,000-10,000' Area (ft^3) [x 10^6]	9,000-10,000' Volume (ft^2) [x 10^9]	13,000-14,162' Area (ft^2) [x 10^6]	13,000-14,162' Volume (ft^3) [x 10^9]	Area total (ft^2) [x 10^6]	Volume total (ft^3) [x 10^9]	Method of determination
White Branch	Snow patch	--	--	3.1	--	1.9	--	.3	--	--	--	5.3	.3	B
	Renfrew	--	--	.3	--	5.2	--	.5	--	--	--	6.	.4	B
	Collier	--	--	3.1	.2	7.9	.5	.4	.005	--	--	11.4	.7	M
	Subtotal	--	--	6.5	--	15.0	--	1.2	--	--	--	22.7	1.4	--
Area Total		.1		26.6		52.3		9.2		1.1		89.3		
Volume Total													5.6	

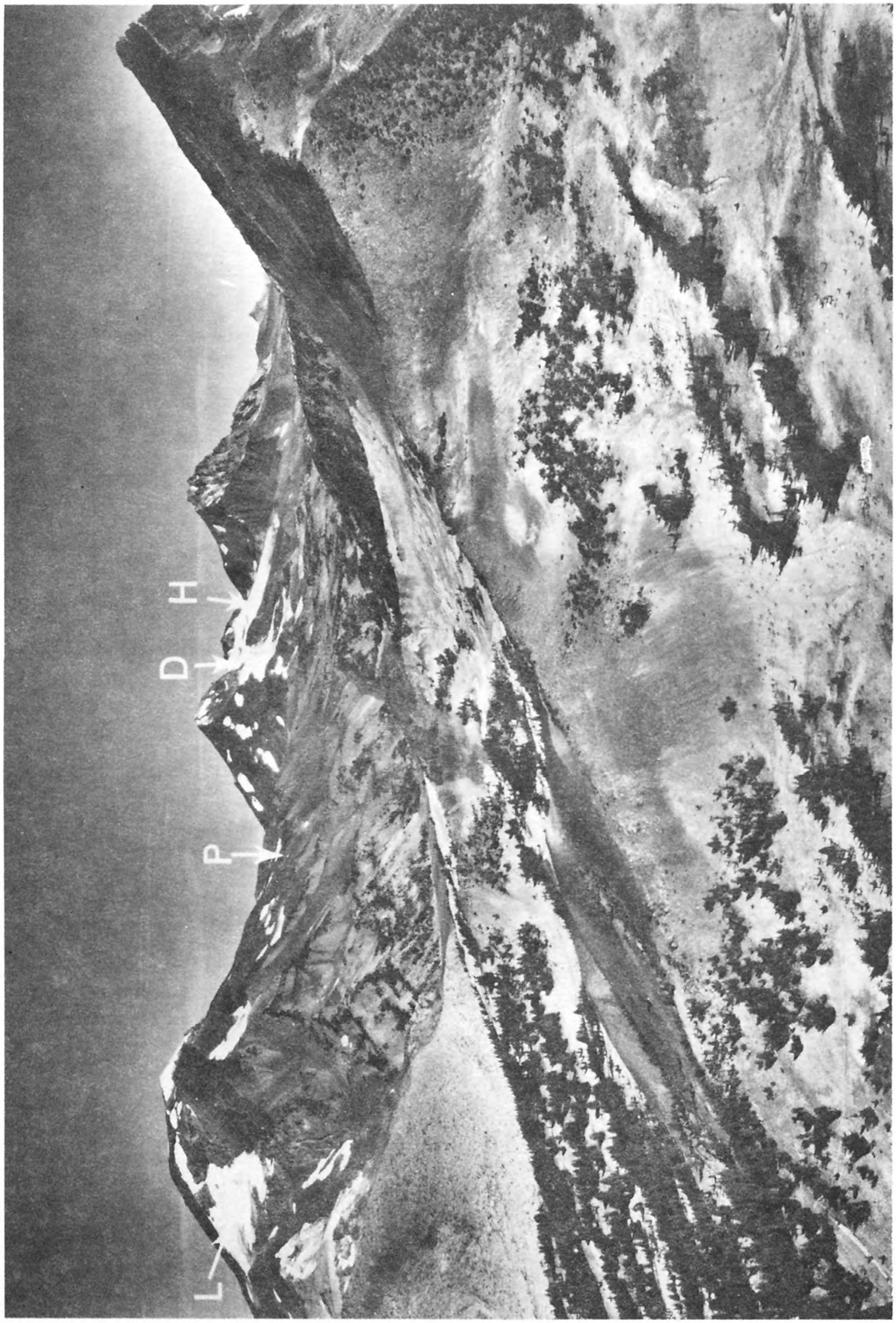

Figure 16.--South, Middle, and North Sisters, and the slope of Broken Top, as seen, left to right, from the southeast. Lewis (L) and Prouty Glaciers are visible on slopes of South Sister. Diller (D) and Hayden (H) Glaciers are visible on right flank of Middle Sister. Most recently erupted lava of 2,000 to 3,000 years ago is visible on the south flank of South Sister. U.S. Geological Survey photograph by Robert Krimmel on August 18, 1981.

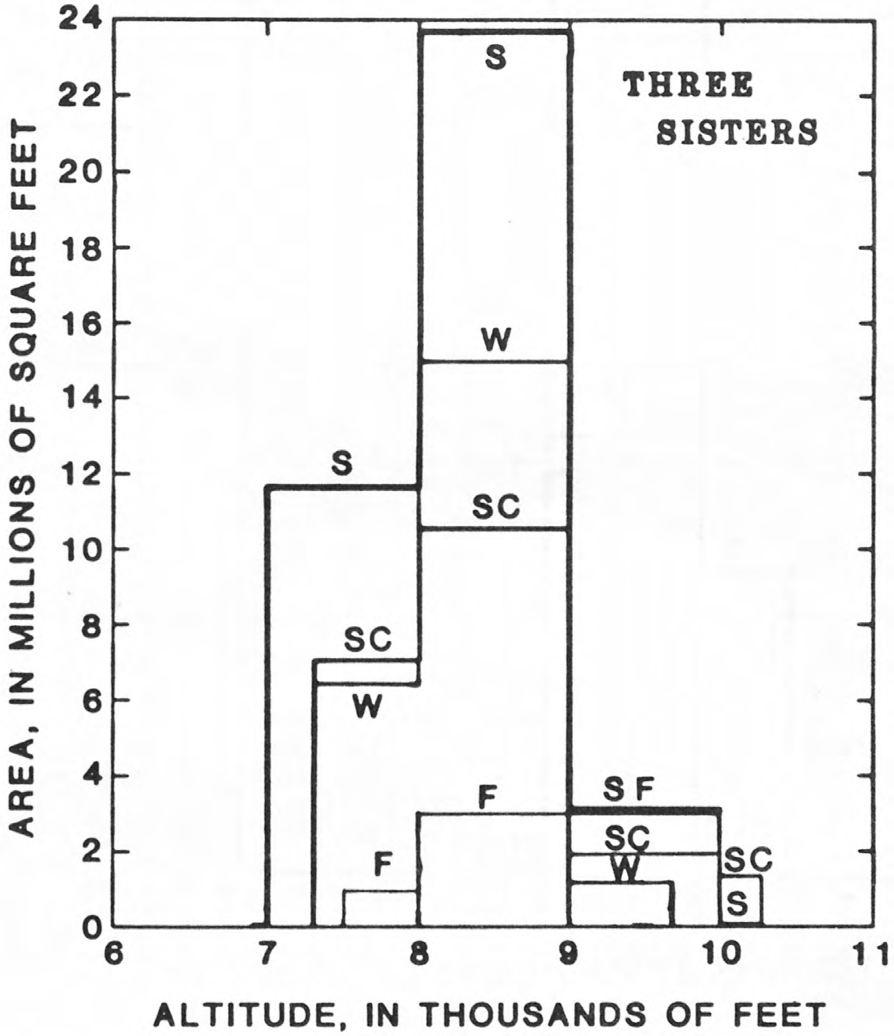

Figure 17.

Figure 17.--Areas of ice and snow in the Three Sisters drainage basins as a function of altitude. Drainage basins listed are as follows: F, Fall Creek; S, Separation Creek; Sc, Squaw Creek; W, White Branch.

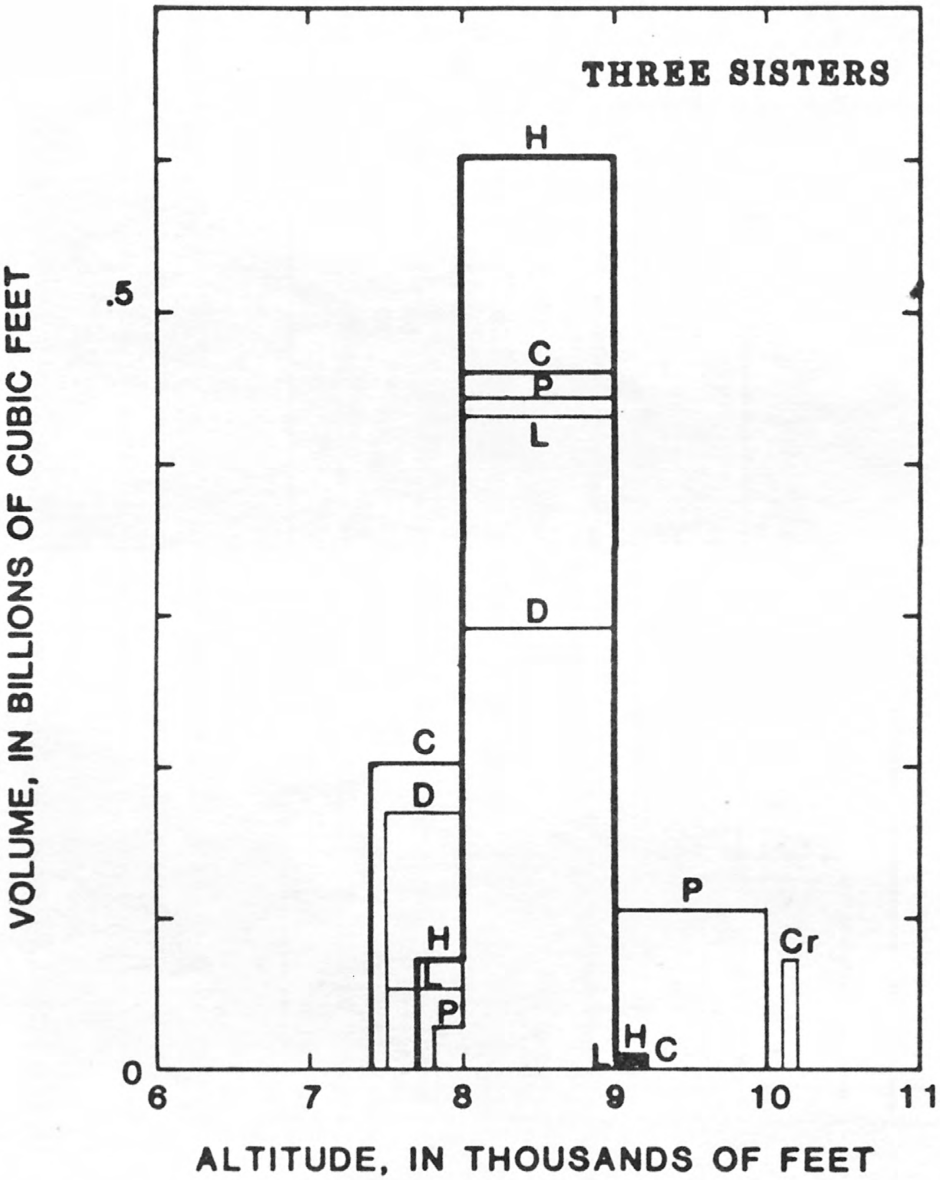

Figure 18.

Figure 18.--Ice volumes on measured glaciers of the Three Sisters volcanoes as a function of altitude. Glaciers listed are as follows: C, Collier on North Sister; Cr, Crater on South Sister; D, Diller on North Sister; H, Hayden on North Sister; L, Lost Creek on South Sister; P, Prouty on South Sister.

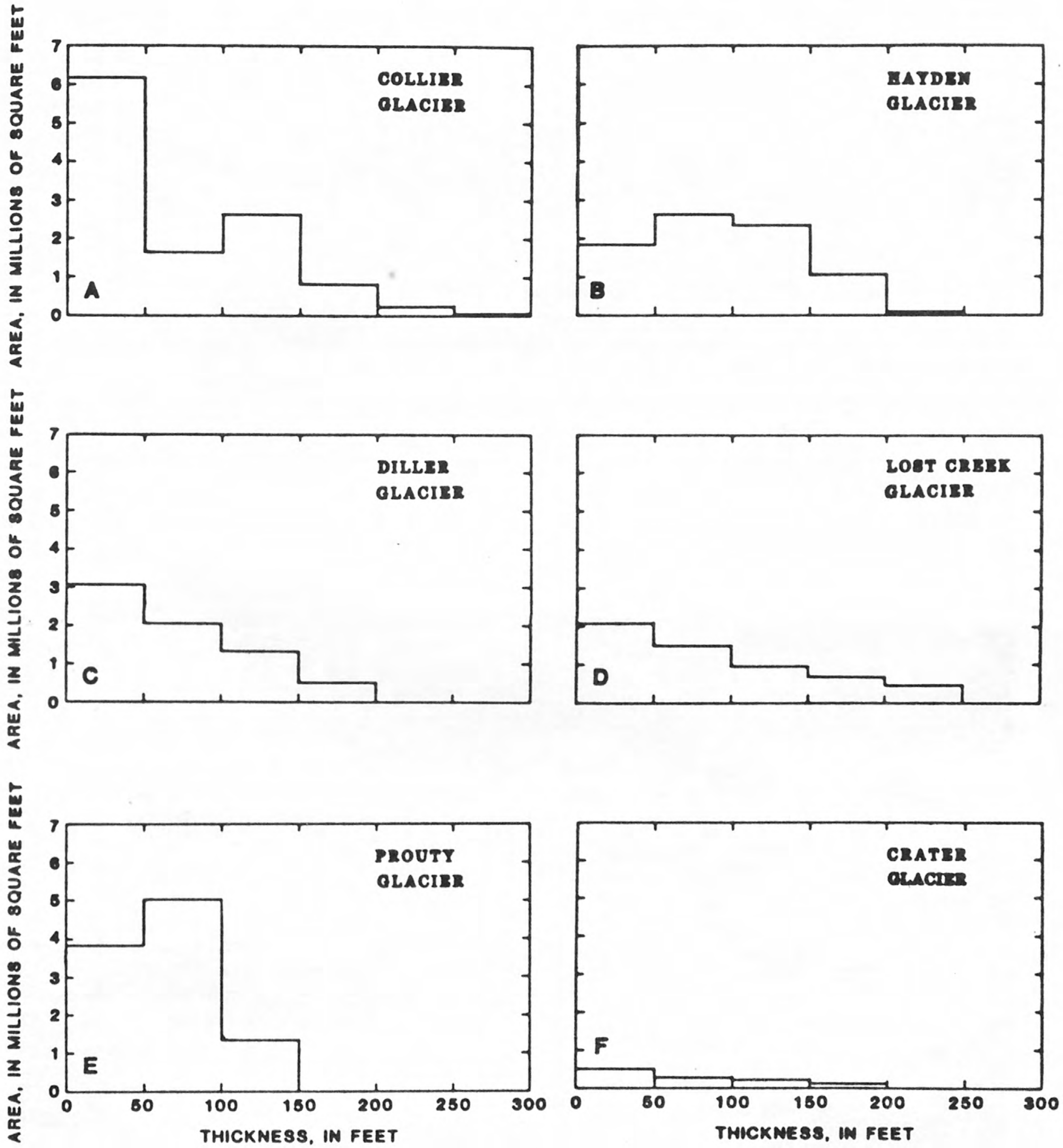

Figure 19

Figure 19A-F.--Areas of ice for selected thickness intervals on radar-measured glaciers of the Three Sisters volcanoes. Values are derived from isopach maps.

Regional eruptive patterns during the Holocene indicate that future rhyodacitic eruptions accompanied by small pyroclastic flows and tephra could occur on the south flank of South Sister in the presence of seasonal snow cover and glacier ice. Figure 17 illustrates that forty-seven percent of the area covered by snow and ice is on the South Sister. In this drainage basin are the Prouty and Lewis glaciers, with a total volume of 0.8 billion ft^3. Basaltic eruptions north and south of the Sisters could pose an additional hazard if erupted on to thick snowpack.

More information on the geology of the Three Sisters volcanic region is available in the recent report by Taylor, (1981).

Mount Shasta

Mount Shasta (fig. 20), with an ice volume of 4.7 billion ft^3, is about 40 miles south of the Oregon-California border.

Snowmelt and glacial meltwater flow from Mount Shasta in four major drainage systems and are shown on plate 6A. Beginning as several intermittent creeks, the south branch of the Klamath River drains Mount Shasta, including the Whitney Glacier. Thirty-nine percent of the area covered by snow and ice is in the Klamath River watershed. The massive volcano is drained on the northeast side by several intermittent creeks, which enter a small closed depression southeast of Whaleback Mountain. Numerous creeks drain the mountain's southeast side and enter the McCloud River, which flows south to the Sacramento River. The southwest sides of Mount Shasta and satellite cone of Shastina are in the Sacramento River drainage area, where several intermittent streams drain the region before disappearing into the porous volcanic rocks above the town of Mount Shasta.

Though the main lobe of the Hotlum Glacier is the largest in area (19.4 million ft^2), and in volume (1.3 billion ft^3), the thickest ice measured on Mount Shasta is the 126 ft recorded on the Whitney Glacier. Whitney Glacier is the only glacier on Mount Shasta measured successfully by ice radar, and has an area of 14 million ft^2 and a volume of 0.9 billion ft^3 (see table 5). Isopachs for Whitney Glacier are seen in plate 6B.

Mount Shasta is a compound stratovolcano composed of overlapping deposits erupted during a period of several hundred thousand years. Past eruptive events have included dome building, lava flows, pyroclastic flows, mudflows, and some small volume eruptions of tephra. Similar future eruptions could occur near the present summit, or could form new vents such as Shastina, and Black Butte, west of Mount Shasta (Miller, 1980, p. 28).

Unlike the valleys on Mount Rainier, those on Mount Shasta are not of great length, allowing mudflows, lava flows, and pyroclastics to form deposits around the flanks of the mountain rather than many miles distant (Miller, 1980, p. 31).

Lava generally flows in existing valleys and, because of its viscous nature, is limited in areal extent. In Holocene time, lava was erupted most often near the summit and less often from the lower flanks of Mount Shasta. Past lava flows have been thick and blocky, and have rarely extended more than 5 miles from their source in the presence of some snow and ice.

Pyroclastic flows, with the potential for covering large areas of ice and snow, have been frequent in the last 10,000 years and have flowed as far as 12

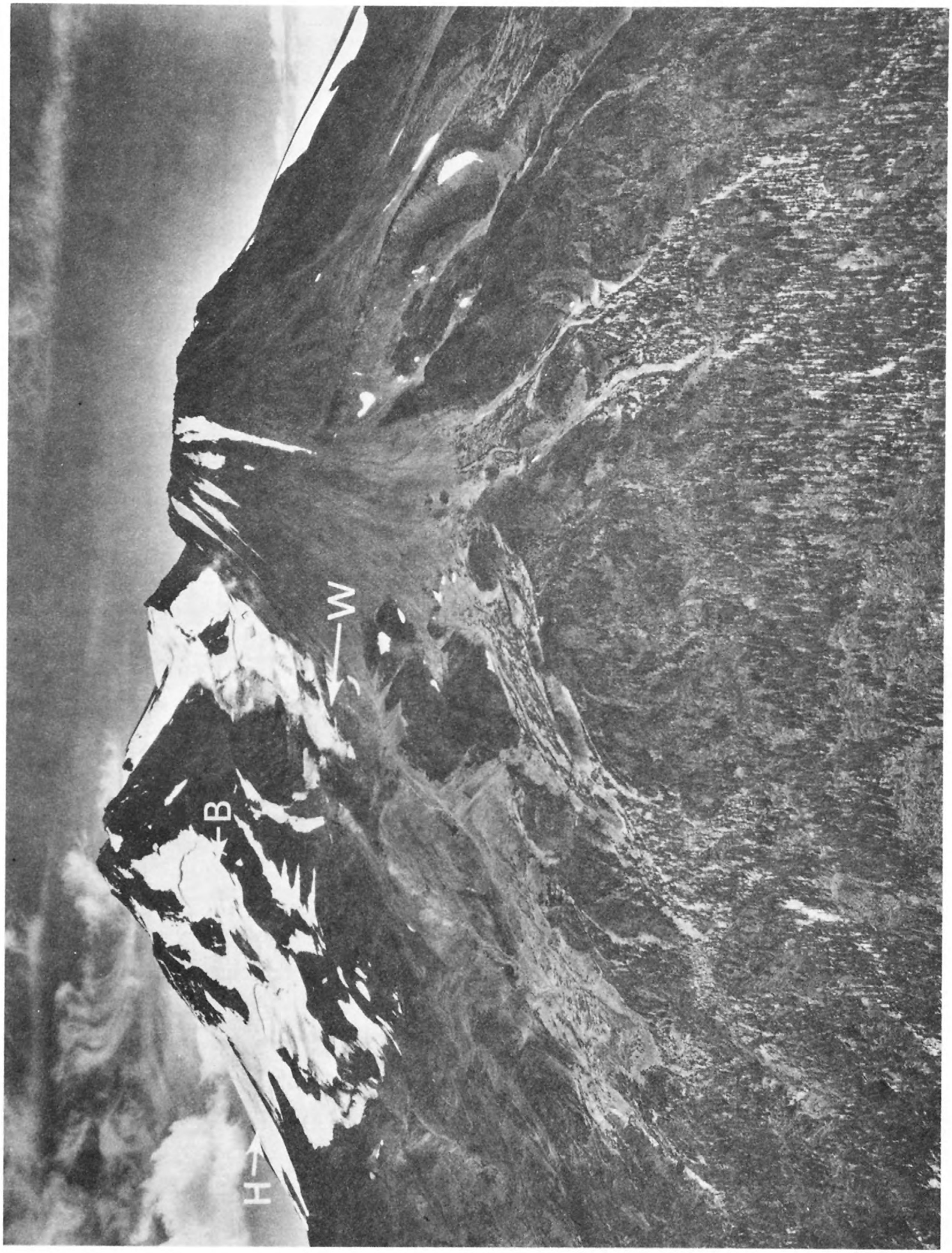

Figure 20.--Mount Shasta, as seen from the northwest. W indicates the Whitney Glacier which flows between Mount Shasta and Shastina on the right. B and H indicate locations of the Bolan and Hotlum Glaciers, seen on the left flank of Mount Shasta. U.S. Geological Survey photograph by Robert Krimmel on August 19, 1981.

Table 5.--Areas and volumes of glacier ice and snow on Mount Shasta. Methods of determination = M, glacier thickness measured by ice radar; B, volume estimated with caluclation of basal shear stress; A, volume estimated using area correlation.

Drainage area	Glacier or snow patch	Altitude Interval										Area total (ft^2) [x 10^6]	Volume total (ft^3) [x 10^9]	Method of determination
		9,000-10,000'		10,000-11,000'		11,000-12,000'		12,000-13,000'		13,000-14,162'				
		Area (ft^2) [x 10^6]	Volume (ft^3) [x 10^9]	Area (ft^2) [x 10^6]	Volume (ft^3) [x 10^6]	Area (ft^2) [x 10^6]	Volume (ft^3) [x 10^9]	Area (ft^3) [x 10^6]	Volume (ft^2) [x 10^9]	Area (ft^2) [x 10^6]	Volume (ft^3) [x 10^9]			
Valley Basin	Snow patches	--	--	.7	--	--	--	--	--	--	--	.7	.05	B
	Hotlum #1	--	--	4.0	--	6.2	--	3.4	--	.8	--	14.4	1.0	B
	Subtotal	--	--	4.7	--	6.2	--	3.4	--	.8	--	15.1	1.1	
Klamath	Snow patches	.7	--	1.9	--	1.3	--	--	--	--	--	3.9	.2	B
	Bolam	.1	--	3.5	--	5.0	--	2.3	--	.5	--	11.4	.8	B
	Whitney	.2	1.4	5.0	292.0	2.7	188.97	2.9	276.8	3.0	158.8	13.8	.9	M
	Subtotal	1.0	--	10.4	--	9.0	--	5.2	--	3.5	--	29.1	1.9	
Sacramento	Snow patches	--	--	1.3	--	3.5	--	1.5	--	.5	--	6.8	.3	B
	Subtotal	--	--	1.3	--	3.5	--	1.5	--	.5	--	6.8	.3	
McCloud	Snow patches	.4	--	.8	--	--	--	.2	--	--	--	1.4	.07	B
	Hotlum #2	--	--	1.3	--	2.4	--	1.1	--	.2	--	5.0	.3	B
	Winton	1.0	--	2.8	--	4.7	--	3.1	--	1.6	--	13.2	.9	B
	Konwakiton	--	--	--	--	.4	--	1.4	--	1.4	--	3.2	.2	B
	Subtotal	1.4	--	4.9	--	7.5	--	5.8	--	3.2	--	22.8	1.4	
Area Total		2.4		21.3		26.2		15.9		8.0		74.0		
Volume Total													4.7	

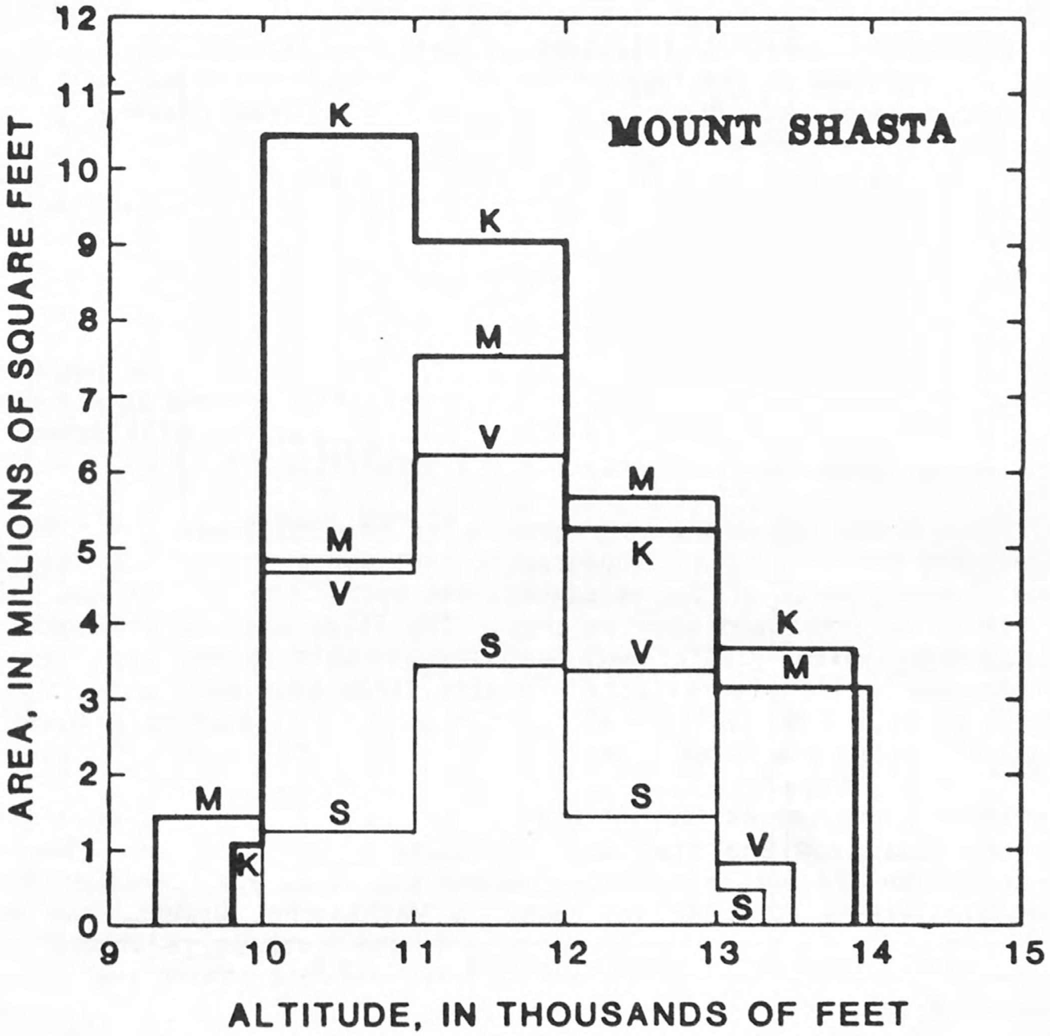

Figure 21.

Figure 21.--Areas of ice and snow in each drainage basin of Mount Shasta as a function of altitude. Drainage basins listed are as follows: K, Klamath; M, McCloud; S, Sacramento; V, a valley basin near the Whaleback Mountain.

miles from their source (Miller, 1980, p. 14). Though their extent depends upon the composition of gas in the eruption, it is probable they will flow over snow and ice.

Floods are common events during volcanic eruptions because of snow and ice-melt. Those originating on volcanoes may be more damaging than floods elsewhere due to their high sediment concentration. Mudflows, many unrelated to eruptions, have traveled more than 16 miles from the summit of Mount Shasta in the valleys of Mud, Ash, Whitney, and Bolam Creeks, and in the valleys of the McCloud and Sacramento Rivers. Figure 21 illustrates that the largest volumes of Mount Shasta's ice are perched at the tops of these drainages, on the northern and eastern parts of the mountain. Ninty-four percent of the area covered by snow and ice is above 10,000 feet of altitude.

More information about geological hazards at Mount Shasta can be found in the report by Miller, 1980.

CONCLUSIONS

On each of the mountains studied substantial amounts of snow and ice exist within probable eruptive zones and should be considered as factors in all eruption-hazard analyses. In times of eruption their role as hazards will depend on the extent of seasonal snow cover and eruption characteristics.

Glacier sizes and locations vary greatly on the volcanoes depending on the local climate and each mountain's topographic configurations. Mount Rainier, the highest and farthest north of the volcanoes, has by far the largest and most well developed valley glaciers and snow patches. The Three Sisters and Mount Shasta have only one major valley glacier each--Collier and Whitney Glaciers, respectively. Mount Rainier's size is reflected in it's large snow and ice volume (155.8 billion ft^3), when compared to those of Mount Hood (12.2 billion ft^3), Mount Shasta (4.7 billion ft^3), and the Three Sisters (5.6 billion ft^3).

The methods of volume estimation used in this study were developed using relationships derived from the ice-radar measurements of glaciers. The methods have been tested on glaciers with known volume and found applicable and valuable for use on glaciers of Cascade volcanoes in Washington, Oregon, and Northern California. However, because glacier area and shear stress relations may vary with climate, it is important that care be taken in determining the suitability of the methods to glaciers elsewhere. The choice of whether to use an area or a basal shear stress correlation is as important as determining the geographical suitability of a glacier. Glaciers not well defined in length and continuity may require some forethought and preliminary estimations of volumes before final estimations are made.

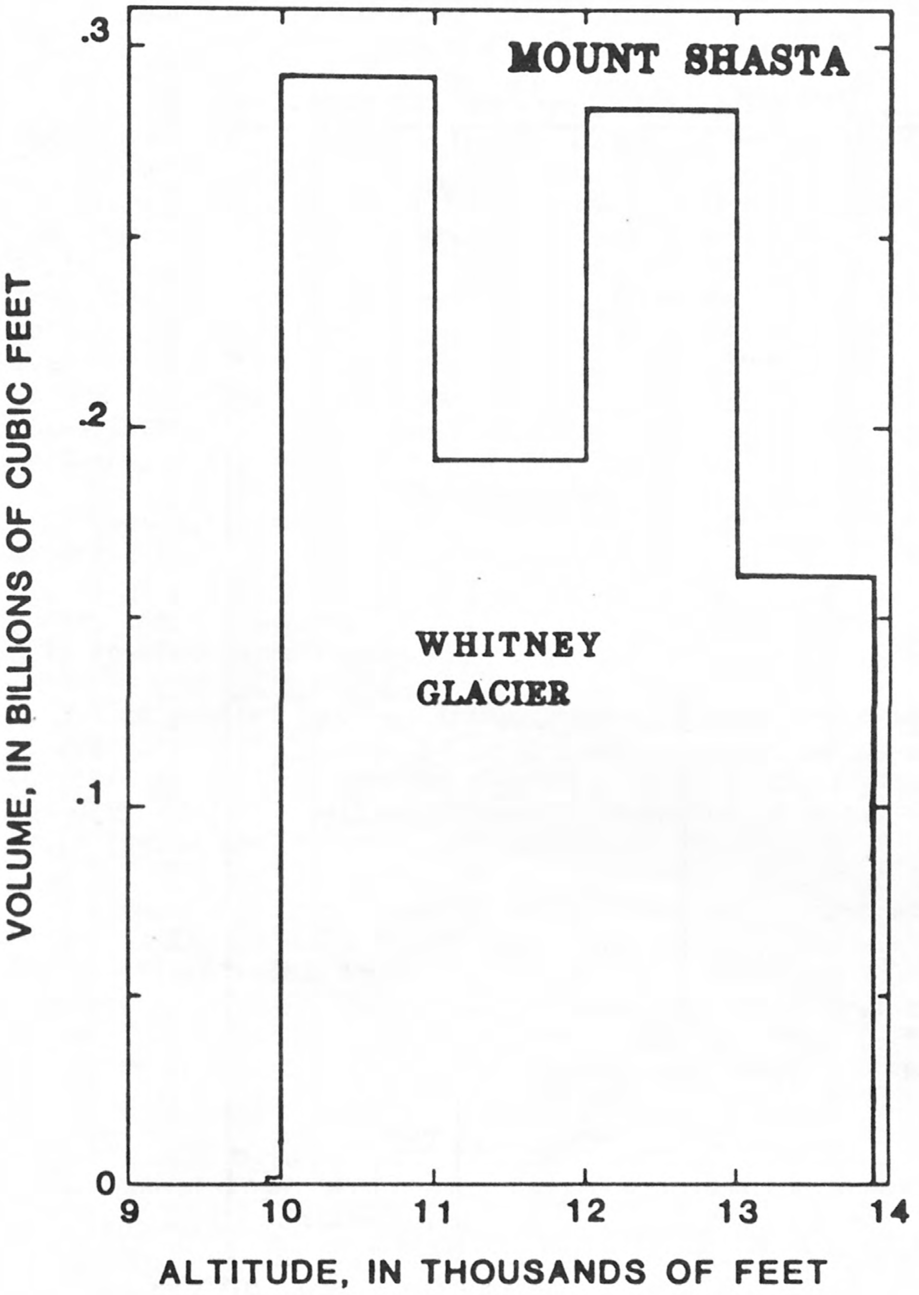

Figure 22.

Figure 22.--Volume as a function of altitude on Whitney Glacier, the only glacier measured successfully by radar on Mount Shasta.

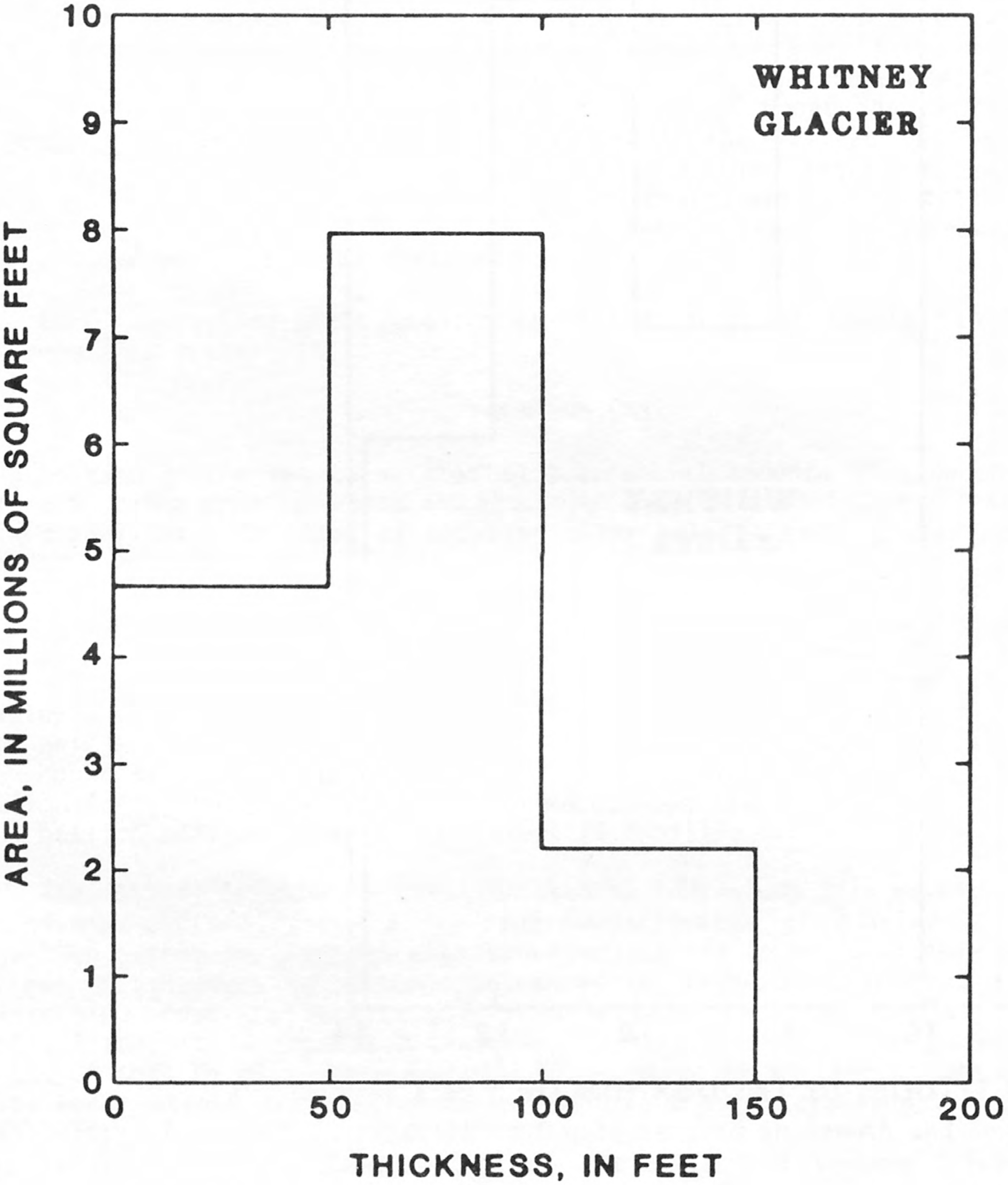

Figure 23.

Figure 23.--Area of ice for selected thickness intervals on Whitney Glacier. Values are derived from isopach map.

APPENDIX

Monopulse Radar - Theory

The comparatively extreme electrical resistance and homogenous nature of ice has allowed successful radar sounding through several miles of polar ice (Fitzgerald and Peran, 1975, p. 39). Until recently, similar success had eluded researchers in their efforts to sound temperate glaciers (where the ice is at the pressure melting point everywhere). The main problem encountered is the scattering caused by water found in temperate glaciers, and not increased electromagnetic absorption in the ice due to higher temperatures. Thus, the signal-to-noise ratio can not be increased by improving system performance (Smith and Evans, 1972, p. 133). The ratio of radio wavelength to effective scatterer radius is recognized to be the controlling factor, and theoretical analysis shows that, if scattering is to be brought down to an acceptable level, the frequency must be reduced to 5 MHz or lower (Watts and England, 1976, p. 46).

Conventional radio detectors are tuned receivers, measuring a rectified electric field at a single frequency as a function of time. Therefore, several cycles of the carrier frequency need to be received in order to generate a response. As a frequency of 5 MHz corresponds to a wavelength of more than 100 ft, this resolution is inadequate for many temperate glaciers.

This problem can be circumvented in theory, by use of a monopulse source at the correct frequency and an untuned receiver, which measures an unrectified electric field as a function of time. In this way, arrival times of the reflected wave could be picked within the accuracy of a small fraction of a single cycle (Watts and England, 1976, p. 40).

The technical breakthrough in application of these ideas was achieved by Roger S. Vickers and R. Bollen and tested by them at South Cascade and Columbia glaciers (Vickers and Bollen, 1974, p. 2). Nondestructive avalanche transistor transmitters provided the necessary monopulse, and resistively loaded antennas eliminated the resonance problem (Watts and England, 1976, p. 40). Subsequent refinements resulted in the portable field unit used in this study.

Monopulse Radar - Application

A thorough treatment of a similar system has been published (Watts and Wright, 1981), so only a basic outline of the instrument circuitry is provided, except where differences merit detail.

The principal components of the ground-based monopulse radar are schematically depicted in figure 24.

The two power supplies consist of 12-volt, rechargeable battery cells with gelatinized electrolyte. Of the two main parts, the receiving oscilloscope has the heavier power requirement, but in no instance was more than one battery change in a working day needed.

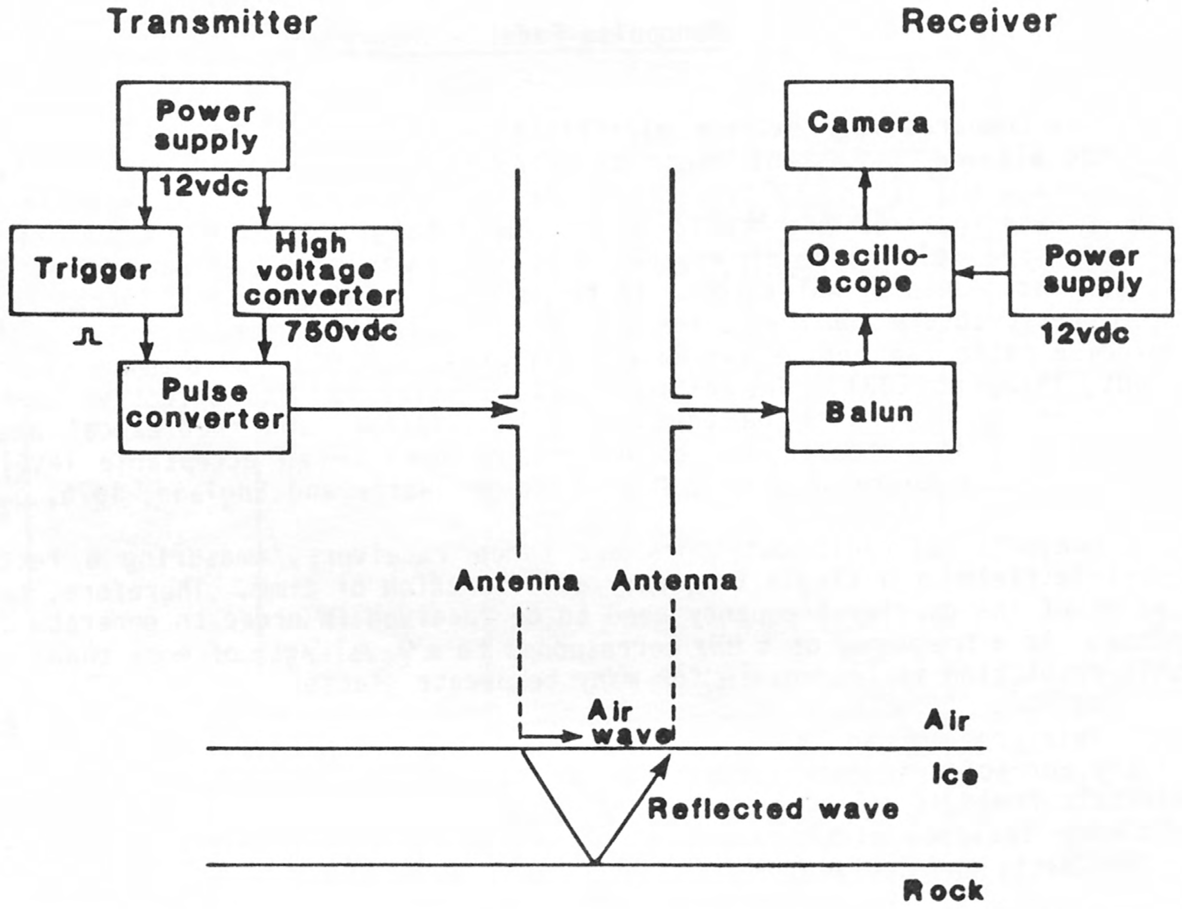

Figure 24.

Figure 24.--Schematic diagram of the radar system (Kennard, 1983).

The specific transmitting circuitry was designed by David Wright, modified by Steven Hodge, and built by Robert Jacobel under the auspices of the Geological Survey. Circuit diagrams are available from the Geological Survey's Project Office - Glaciology. The antenna design was done by G. C. Rose and R. S. Vickers (1974, p. 261) and modified for field use by Steven Hodge (U.S. Geological Survey, written commun., October 1978).

The transmitter power supply energized a trigger circuit and a high-voltage, direct-current source. The trigger controlled the repetition rate (as distinct from the frequency) of the transmitted monopulse. This rate was variable over two ranges, 0.1 to 12.8 kHz. The oscilloscope recorded both the transmitted (air) wave, returns from intraglacial scattering, and the reflection from bedrock. Thus, the repetition rate needed regulation so that a subsequently transmitted wave would not obscure an earlier reflected wave.

The brightness of the oscilloscope trace is proportional to the repetition rate, which is an important factor in a sunlit field situation. Power consumption was increased with higher pulse rates, but still never approached that of the receiver. A repetition rate of 10 kHz was generally used.

The power supply was a low to high voltage converter that supplied the necessary power for the transmitted pulse. A 750-volt, -20 mA capacity converter sufficed for the pulse generator configuration at the repetition rates used.

The pulse generator consisted of a variable number of avalanche transistor stages. Increasing the number of stages increased the amplitude of the transmitted pulse, until it was limited by the high-voltage supply and the thermal-dissipation capabilities of the transistors. Three configurations were tested -- low power (2 stage), medium power (3 stage), and high power (4 stage). The optimal unit for these studies seemed to be the medium power pulse, which produced 600 volt pulses into a 50 Ω load. The low-power unit produced approximately 40-percent less power (Jacobel and Raymond, 1984), but caused no problem when used in the field. The high-power unit did not produce significantly more output, but drew more current.

When a stage avalanched, it produced a fast voltage rise time (several tens of nanoseconds), and then returned to a high impedance state. The discharge current was limited by the antenna impedance, so the avalanching was nondestructive.

The final component of the transmitter system was the resistively loaded antenna, which was identical to the receiving antenna. The center frequency of the transmitted pulse (limited by the pulse generator) is a function of the antenna length and a resistive loading constant (Ψ). When the antenna is lying on an ice surface, the frequency is given approximately by the equation,

$$\nu = 50/\ell \quad , \tag{1}$$

where ν is in megahertz and ℓ is the antenna half-length in meters.

To prevent ringing of the pulse produced by the transmitter the antenna is loaded according to the relation,

Figure 25.--Antenna detail (diagram illustrates positioning of resistors in the radar antenna. Diagram from written communication, S. M. Hodge, U.S. Geological Survey, October 1978).

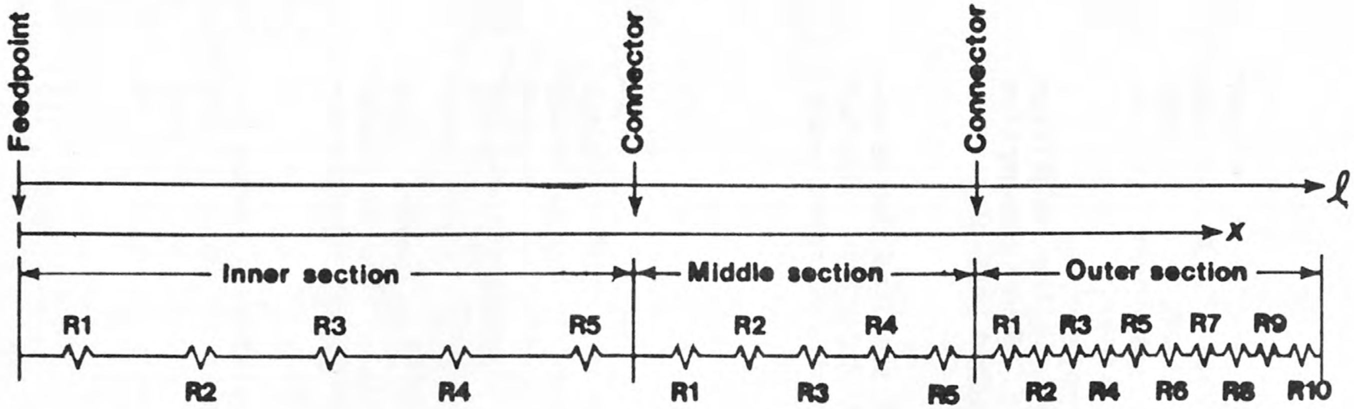

To determine the required values of resistors in the outer antenna section, the antenna is divided into 10 intervals. Resistance is calculated where

$$\Delta R_{ab} = \int_a^b (\psi/Z)dZ = \psi \ln Z\Big|_b^a$$

$Z = \ell - x$, where ℓ is the antenna halflength, and x is the distance from the antenna feedpoint. R values for the inner middle sections equal values for R1-R5 in the outer section. Halflengths for high and low frequency antennas are shown below.

Halflengths of antenna in meters

Section	Low frequency	High frequency
Inner	20	2.5
Middle	10	1.25
Outer	10	1.25

(Antenna detail adopted from communication, S.M. Hodge, U.S. Geological Survey, October 1978).

Figure 25. ANTENNA DETAIL

$$R(x) = \Psi/(\ell - x) \quad , \tag{2}$$

where R is resistance per unit length at distance x from the feed point, and Ψ is a constant in ohms. The constant, Ψ, affects the pulse duration and the radiated power. Increasing Ψ decreases the duration of the pulse (increasing resolution), but also decreases the radiated power. In practice, the variation is not critical, and in applications where increased power is needed such as in thick ice, the decrease in resolution is usually acceptable.

The two main criteria for antenna design are the length, which determines frequency and the resistive loading, which determines resolution and power. In this study, two basic configurations were chosen with respect to frequency: the "high" and the "low". Because frequency is a function of antennas length only, it can be changed by simply removing or adding center sections of the antenna. If the section lengths are chosen as shown in figure 25, only 10 discrete resistor values are required for a given Ψ value, and one antenna design is thus capable of producing pulses at six different frequencies (Steven Hodge, U.S. Geological Survey written commun., October 1978).

The antennas used on the project were Ψ = 400 Ω (low frequency) and Ψ = 1500 Ω and 2500 Ω (high frequency). In testing antennas, it has been found that the outer arms alone (10 m, 5 MHz) of the low frequency antennas give the best results on the relatively thin, temperate glaciers of the Cascade Range, and were the easiest to operate. These tests were not comprehensive, yet it was found that, if a good bottom reflection could not be achieved with the "low-frequency" set, it could not be achieved with the "high-frequency" set. This result was not surprising, considering the expected signal scattering in temperate glaciers. Generally, in this study the 400 Ω antennas were used.

The transmitted signal was about 10^6 times stronger than the received signal, necessitating the use of separate but identical antennas. The receiving antenna impedance was matched to the oscilloscope with a balun. Optimal input:output voltage and impedance ratios (Hodge, U.S. Geological Survey, written commun., October 1978) were found to be 3:1 and 9:1, respectively. Others have also used a preamplifier (for thick ice) and a bandpass filter (1-10 MHz) at this stage (Watts and Wright, 1981, p. 460), though these were not required in this fieldwork.

The oscilloscope constitutes the core of the receiving system. A band width of 30 MHz is used, and the unit is otherwise chosen according to power requirements, weight, sensitivity, and trace brightness.

The oscilloscope trace is triggered by the incoming air wave and records this wave and the reflected wavelet (fig. 26). A two-channel oscilloscope is preferable because the incoming signal can be viewed at two different amplification levels. In this way, a relatively strong air wave and a reflected wave can be viewed in detail simultaneously.

The trace output was recorded by an oscilloscope camera on self-developing film. Minimization of light leaks and maintaining the film at higher-than-ambient temperature were the only difficulties encountered.

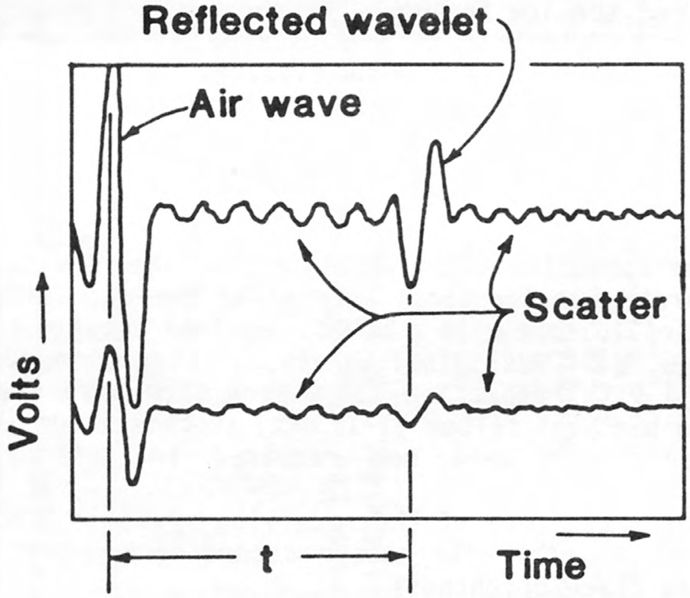

Figure 26.

Figure 26.--Oscilloscope output. Air wave and reflected wavelet as seen on the oscilloscope screen. Quick developing photographs were taken of the traces at each measurement point. The time interval between wave transmission and receival is expressed as t. Two traces were set at differing amplitudes to accent features in the air wave and the reflected wave.

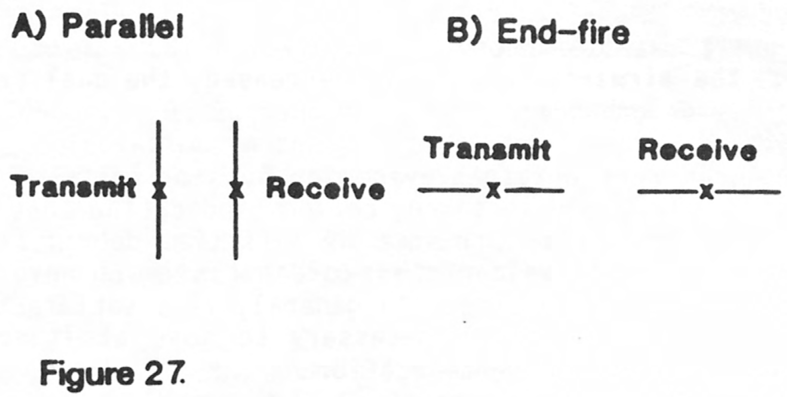

Figure 27.--Diagram shows typical antenna configurations used during measurements. Placement was dependent on the clarity of a bottom return on the oscilloscope trace.

The layout geometry of the antenna at each measurement point depended on the ability of a particular configuration to give an unambiguous bottom return. Figure 27 shows the primary antenna layouts used on the glacier. In general, the parallel configuration (A) was tried first. The air-wave used to trigger the scope is of predictable polarity and there is maximum coupling of the antennas. An attempt was made to align the antennas parallel to the expected bottom contours. If ambiguous returns continued, the separation distance between the transmitter and receiver antenna was changed.

If bottom returns were still unsatisfactory, configuration (B) was used at various separations. Although the airwave coupling is decreased, the quality of bottom returns would occasionally be enhanced.

Some successful bottom returns were obtained even with both or parts of the antennas hanging down crevasses, and, in one instance, coiled, indicating that the antenna configuration was not critical. The presence of surficial debris, crevasses of various orientations, water, or volcanic ash did not seem to have any effect on the success of receiving bottom returns. In general, if a satisfactory bottom return was not found in an area, it was necessary to move at least an antenna-length away from the original measurement location.

The hard copy of the data was a photograph of the oscilloscope trace as seen in figure 26. As the air wave triggers the oscilloscope, it is necessary to know the transmitter-receiver separation in order to determine the total travel time of the reflected wave. First seen on the left side of the scope trace is the air wave.

A surface wave also travels directly through the ice and usually appears as a minor disruption of the air wave. Next are returns of scattered signals from ice inhomogenieties, finally followed by the reflected wave, which has undergone a phase reversal.

For depth determination, the information of interest is the time delay (t) between a point on the airwave and a corresponding point on the reflected wave. Because frequency is not necessarily preserved between the air and reflected waves, it is most accurate to choose this point to be early along the pulse. Almost exclusively the first peak was chosen (whether of positive or negative amplitude) to be the basis for calculation of the time delay.

For purposes of this study, the only concerns were the respective positions of the air and reflected waves. It is possible that useful information about the nature of englacial scatterers can be obtained from further study of the remainder of the recorded signals (Jacobel and Raymond, 1984).

References Cited

Brückl, E., 1973, Methoden zur berechnung des Eis Volumens an Gletschern: Vortrag gehalten am 9th International Polar Meeting in München, 25-27 April, 1975, (unveröffentlicht).

Brugman, M. M., and Post, Austin, 1981, Effects of volcanism on the glaciers of Mount St. Helens: U.S. Geological Survey Circular 850 D, 11 p.

Crandell, D. R., 1971, Postglacial lahars from Mount Rainier volcano, Washington: U.S. Geological Survey Professional Paper 677, 73 p.

Crandell, D. R., and Miller, R. D., 1974, Quaternary stratigraphy and extent of glaciation in the Mount Rainier region, Washington: U.S. Geological Survey Professional Paper 847, 59 p.

Crandell, D. R., 1980, Recent eruptive history of Mount Hood, Oregon, and potential hazards from future eruptions: U.S. Geological Survey Bulletin 1492, 81 p.

Crandell, D. R., and Mullineaux, D. R., 1981, Volcanic hazards at Mount Rainier, Washington: U.S. Geological Survey Bulletin 1238, 26 p.

Fitzgerald, W. J., Paren, J. G., 1975, The dielectric properties of Antarctic Ice, Symposium on remote sensing in Glaciology: Journal of Glaciology, v. 15, no. 73, p. 39-48.

Heliker, C. C., Johnson, Arthur, and Hodge, S. M., 1983, The Nisqually Glacier Mount Rainier, Washington, 1857-1979: U.S. Geological Survey, Open File Report 83-541, 20 p.

Jacobel, Robert, and Raymond, Charles, 1984, Radio-echo sounding studies of englacial water movement in Variegated Glacier, Alaska: Journal of Glaciology, v. 30, no. 103 [In press].

Kennard, P. M., 1983, Volumes of glaciers on Cascade volcanoes: Seattle, Wash., University of Washington, unpublished thesis, 151 p.

Kotliatov, V. M., 1980, Problems and results of studies of mountain glaciers in the Soviet Union: Proceedings of the Riederalp workshop, Internationa Association of Scientific Hydrology, no. 126, p. 129-137.

Macheret, Yu., Ya., Zhuravlev, A. B., 1982, Radio echo-sounding of Svalbard glaciers: Journal of Glaciology, v. 28, no. 99, p. 295-314.

Miller, C. D., 1980, Potential hazards from future eruptions in the vicinity of Mount Shasta volcano, northern California: U.S. Geological Survey Bulletin 1503, 25 p.

Müller, F., Caflisch, T., and Müller, G., 1976, Firn und Eis der Schweizer Alpen (Gletscher Inventar): Institute of Geography, Swiss Federal Institute of Technology, pub. 57, 293 p.

Nye, J. F., 1951, The flow of glaciers and ice-sheets as a problem in plasticity: Proceedings of the Royal Society of London, A, v. 207, p. 554-572.

___1952, A method of calculating the thickness of the ice-sheets, Nature, v. 169, p. 529-533.

Paterson, W. S. B., 1970, The application of ice physics to glacier studies: in Glaciers, Proceedings of workshop seminar, Canadian National Committee for Hydrological Decade, p. 43-46.

___1981, The physics of glaciers: New York, Permagon Press, p. 83-89.

Post, A., Richardson, D., Tangborn, W., Rosselot, F., Inventory of glaciers in the North Cascades,m Washington: U.S. Geological Survey Professional Paper 705-A, 26 p.

Rose, G. C., and Vickers, R. S., 1974, Calculated and experimental response of resistively loaded V antennas to impulsive excitation: International Journal of Electronics, v. 37, no. 2, p. 261-271.

Shih Ya-Feng, Wang Zongtai, Liu Chaohai, 1981, Progress and problems of glacier inventory in China: Zeitschrift für Gletscherkunde und Glazialgeologie, v. 17, no. 2, p. 191-198.

Smith, B. M. E., and Evans, S., 1972, Radio echo sounding: absorption and scattering by water inclusion and ice lenses: Journal of Glaciology, v. 11, no. 61, p. 133-146.

Taylor, E. M., 1981, Roadlog for central high Cascade geology Bend, Sisters, McKenzie Pass, and Santiam Pass, Oregon, in Johnston, D. A., Donnelly-Nolan, Julie, eds., Guides to some volcanic terranes in Washington, Idaho, Oregon, and Northern California: U.S. Geological Survey Circular 838, p. 59-84.

Vickers, R. S., Bollen, R., 1974, An experiment in the radio echo sounding of temperate glaciers: Stanford Research Insititute final report prepared for U.S. Geological Survey, 16 p.

Watts, R. D., and England, A. W., 1976, Radio echo sounding of temperate glaciers: ice properties and sounder design criteria: Journal of Glaciology, v. 17, no. 75, p. 39-48.

Watts, R. D., and Wright, D. L., 1981, Systems for measuring thickness of temperate and polar ice from the ground or from the air: Journal of Glaciology, v. 27, no. 97, p. 459-469.

Williams, Howel, 1944, Volcanoes of the Three Sisters region, Oregon Cascades: Berkeley, University of California, 46 p.

Wise, William S., 1969, Geology and petrology of the Mount Hood area: a study of High Cascade volcanism: Geological Society of America Bulletin, v. 80, no. 6, p. 969-1006.

Wozniak, K. C., and Taylor, E. M., 1981, Late Pleistocene summit construction and Holocene flank eruptions of South Sister volcano, Oregon: EOS, Transactions of the American Geophysical Union, v. 62, no. 6, p. 61.

Zhuravlev, A. B., 1980 Opredelenige ob"yema gornykhy lednikov po dannym radiozondirovaniya s vertoleta [the determination of volume of mountain-type glaciers from radio-echo sounding data from helicopters]: Materialy Glyatsiologischeskikh Issledovanig Khronika Obsuzhdeniya, Uyp. 37, p. 140-148.

*GPO 797 - 039 (1984)